

The Effect of Explicit Convection on Couplings between Rainfall, Humidity, and Ascent over Africa under Climate Change

LAWRENCE S. JACKSON AND DECLAN L. FINNEY

School of Earth and Environment, University of Leeds, Leeds, United Kingdom

ELIZABETH J. KENDON

Met Office, Exeter, United Kingdom

JOHN H. MARSHAM

National Centre for Atmospheric Science, and School of Earth and Environment, University of Leeds, Leeds, United Kingdom

DOUGLAS J. PARKER

School of Earth and Environment, University of Leeds, Leeds, United Kingdom


RACHEL A. STRATTON, LORENZO TOMASSINI, AND SIMON TUCKER

Met Office, Exeter, United Kingdom

(Manuscript received 2 May 2019, in final form 7 April 2020)

ABSTRACT

The Hadley circulation and tropical rain belt are dominant features of African climate. Moist convection provides ascent within the rain belt, but must be parameterized in climate models, limiting predictions. Here, we use a pan-African convection-permitting model (CPM), alongside a parameterized convection model (PCM), to analyze how explicit convection affects the rain belt under climate change. Regarding changes in mean climate, both models project an increase in total column water (TCW), a widespread increase in rainfall, and slowdown of subtropical descent. Regional climate changes are similar for annual mean rainfall but regional changes of ascent typically strengthen less or weaken more in the CPM. Over a land-only meridional transect of the rain belt, the CPM mean rainfall increases less than in the PCM (5% vs 14%) but mean vertical velocity at 500 hPa weakens more (17% vs 10%). These changes mask more fundamental changes in underlying distributions. The decrease in 3-hourly rain frequency and shift from lighter to heavier rainfall are more pronounced in the CPM and accompanied by a shift from weak to strong updrafts with the enhancement of heavy rainfall largely due to these dynamic changes. The CPM has stronger coupling between intense rainfall and higher TCW. This yields a greater increase in rainfall contribution from events with greater TCW, with more rainfall for a given large-scale ascent, and so favors slowing of that ascent. These findings highlight connections between the convective-scale and larger-scale flows and emphasize that limitations of parameterized convection have major implications for planning adaptation to climate change.

 Denotes content that is immediately available upon publication as open access.

Corresponding author: Lawrence S. Jackson, l.s.jackson@leeds.ac.uk



This article is licensed under a [Creative Commons Attribution 4.0 license](http://creativecommons.org/licenses/by/4.0/) (<http://creativecommons.org/licenses/by/4.0/>).

DOI: 10.1175/JCLI-D-19-0322.1

© 2020 American Meteorological Society

1. Introduction

The tropical rain belt over Africa is a zone of heavy rainfall that migrates seasonally about the equator between the Northern and Southern Hemispheres. It is arguably the most prominent climate feature over the African continent, accounting for the majority of rainfall in the tropics and central to the distribution of climate zones and their seasonal variation. We follow [Nicholson \(2018\)](#) and refer to the tropical rain belt, rather than the intertropical convergence zone (ITCZ), to unambiguously distinguish the region of intense rainfall and deep convection from the regions of near-surface wind convergence. Over continental Africa, the rains are generally found equatorward of the maximum low-level wind convergence ([Leroux 1998](#); [Nicholson 2009](#)).

The ascending branch of the Hadley cell has upward fluxes of air and moist static energy (MSE) in its mean climatological state. On meteorological timescales, the ascending branch of the Hadley cell comprises mesoscale cloud systems, with areas of convective and stratiform rain, separated by regions of subsidence ([Zipser 1969](#)). Abrupt differences in specific humidity exist between the high humidity of the cloud systems and the relatively low humidity of the subsidence regions ([Williams and Gray 1973](#)). In regions of tropical convection, the vertical temperature profile is close to a moist adiabat from the lower troposphere (not near the surface) to the upper troposphere where specific humidity is low (~ 350 hPa) ([Mapes 2001](#)). The regions of convection within the mesoscale cloud systems include intense convective updrafts of high MSE air that extend from the boundary layer to the upper troposphere (“hot towers”; [Riehl and Malkus 1958](#)). Ascent within these hot towers accounts for the profile of vertical velocity within the cloud systems with its peak velocity in the mid- to upper troposphere ([Williams and Gray 1973](#)).

Under climate change, atmospheric water vapor is expected to be strongly constrained by the Clausius–Clapeyron relationship ([Collins et al. 2013](#)) and therefore increases exponentially with increases in temperature ([Allen and Ingram 2002](#)) at a global rate of $\sim 7.4\% \text{ K}^{-1}$ for total column water vapor and $\sim 5.9\% \text{ K}^{-1}$ for near surface specific humidity ([O’Gorman and Muller 2010](#)). Relative humidity is expected to reduce over land due to its dependency on moisture transport from the oceans ([Byrne and O’Gorman 2018](#)), which are projected to warm less than the land ([Joshi et al. 2008](#)), although there will be regional variations associated with changes in atmospheric circulation and land surface characteristics ([Byrne and O’Gorman 2018](#)). Changes in the Hadley circulation are also projected to change the vertical and zonal distribution of relative humidity within the tropics, most notably drying

the upper regions of the ascending branch (400–150 hPa) and the subsiding branch of the circulation ([Lau and Kim 2015](#)).

The tropical atmospheric circulation is projected to weaken under climate change ([Held and Soden 2006](#); [Chadwick et al. 2013](#)) with weakening of the Walker circulation being more robust in climate model simulations than weakening of the Hadley circulation ([Vecchi and Soden 2007](#)). Several mechanisms have been advanced for the slowing of tropical circulations in response to climate change ([Ma et al. 2018](#)). [Knutson and Manabe \(1995\)](#) argued that weaker ascent in the Walker circulation over the Pacific Ocean could be accounted for by enhanced radiative cooling in the upper troposphere and increased static stability across the tropics balancing an increase in convective heating of the atmosphere. Using a relationship between precipitation, convective mass flux, and humidity, [Held and Soden \(2006\)](#) demonstrated that the convective mass flux has to slow to balance projected increases in precipitation of $\sim 2\% \text{ K}^{-1}$ and humidity of $\sim 7\% \text{ K}^{-1}$. In their mechanism of mean advection of stratification change (MASC), [Ma et al. \(2012\)](#) demonstrate that enhanced tropics wide heating of the upper troposphere acts to stabilize the tropical atmosphere and slow tropical circulations. Slowdown of the tropical atmospheric circulations, however, is contingent on an increase in the depth of convection ([Chou and Chen 2010](#)).

A reduced rate of mean ascent in the ascending branch of the Hadley circulation will be accompanied by pronounced changes in the distribution of vertical velocities. Narrowing of the ascending branch of the Hadley circulation ([Byrne and Schneider 2016](#)) in the form of a “deep-tropics squeeze” will drive pronounced decreases in the rate of ascent along the margins of the ascending branch and intensified rates of ascent within the core of the circulation ([Lau and Kim 2015](#)). Increases in updraft velocities, however, are most likely to occur in the upper troposphere linked, in part, to the increased depth of convection ([Singh and O’Gorman 2015](#)). Recent trends in thunderstorm area and intensity over the Congo basin show that storms have become deeper and more intense while mean rates of ascent have weakened at all levels ([Raghavendra et al. 2018](#)). Uncertainties remain, however, in understanding the mechanisms that drive the change in updraft intensity within the Hadley circulation ([Byrne et al. 2018](#)) and uncertainties in changes of tropical circulations over land remain a salient research gap ([Ma et al. 2018](#)).

Global precipitation is projected to increase under climate change at a rate of $1\%–3\% \text{ K}^{-1}$ coupled with an increase in precipitation intensity and less frequent occurrence of weaker precipitation events ([Collins et al. 2013](#)). Future precipitation change over tropical Africa

remains uncertain for the late twenty-first century (Niang et al. 2014); indeed, drying trends have prevailed over the Congo rain forest since the 1980s (Zhou et al. 2014). Precipitation changes over land will be driven by changes in convergence zones and relative humidity (Chadwick et al. 2013), which, in turn, will be dependent on changes in surface warming patterns that drive the pattern of precipitation change in accordance with the “warmer-get-wetter” hypothesis (Chadwick et al. 2014). Recent convection-permitting simulations of twenty-first century climate over Africa project enhanced wet and dry extremes as well as both sub- and super-Clausius–Clapeyron scaling of precipitation changes at the regional scale (Kendon et al. 2019).

Moist convection is parameterized in climate models to capture subgrid-scale convective ascents and descents but remains one of the largest sources of model error (Sherwood et al. 2014). Global climate models produce rainfall that is less intense but more frequent than observed (Stephens et al. 2010) and regional rainfall changes can be sensitive to the convection parameterization used (Gochis et al. 2002). Climate models with parameterized convection have difficulty capturing the observed timing of the diurnal cycle in convection (Yang and Slingo 2001; Nikulin et al. 2012), the location of convection (e.g., through land–atmosphere coupling; Taylor et al. 2013), and its relationship with low-level moisture convergence (Birch et al. 2014a).

Convection-permitting models (CPMs), in which convection is explicitly resolved at high spatial resolutions, produce improved simulations of rainfall, convection, and atmospheric dynamics compared to parameterized convection models (PCMs) (Prein et al. 2015). They are increasingly being used in operational rainfall forecasting (Clark et al. 2016) and explicitly resolving convection may be necessary to advance understanding of changes in updraft intensity within the Hadley circulation. CPMs are particularly valuable for tropical Africa: the tropical regions of Africa have pronounced diurnal cycles in rainfall that vary regionally and by season (Jury 2016); Africa has varied terrain and land–atmosphere coupling (Koster et al. 2004); and the production of rainfall is dominated by deep atmospheric convection (Schumacher and Houze 2003). Rainfall in CPMs at subdaily time scales is less frequent, more intense, and occurs later in the day than in equivalent PCMs and provides a closer match to observations and satellite data (Pearson et al. 2014; Woodhams et al. 2018; Stratton et al. 2018; Stein et al. 2019; Finney et al. 2019). Westward storm propagation in the latitude band 5°–15°N is better captured (Stratton et al. 2018; Crook et al. 2019) as is the intensity of rainfall extremes (Kendon et al. 2019). Simulations using CPMs over Africa have demonstrated improvements in coupling

between convection and convergence (Birch et al. 2014a) and in capturing the role of the land surface in convective initiation (Taylor et al. 2013). Together with the more realistic propagation and organization of convective systems, CPMs give improved upscale impacts to continental-scale circulations (Marsham et al. 2013; Birch et al. 2014b; Willetts et al. 2017; White et al. 2018; Hart et al. 2018). Further, intermodel differences in the seasonal migration of the tropical rain belt have been shown to be significantly smaller over Africa than other regions in CMIP3 models (Suzuki 2011) and improved in CMIP5 models (Biasutti 2013). This suggests that simulation of the tropical rain belt over Africa is relatively robust in global climate models and insensitive to specific model physics.

This study uses a pan-Africa-scale CPM, building on Stratton et al. (2018) and Kendon et al. (2019), to provide new insights into the response of rainfall and atmospheric circulation to climate change and contribute to a deeper understanding of persistent uncertainties. Our aim is to use the CPM to contrast changes in time-averaged mean climate with changes in the underlying distributions of 3-hourly data, and to examine connections between changes at the convective scale and at large scale. To that end, we analyze the relationships between rainfall, vertical velocity (at 500 hPa), and total column water (TCW) in the ascending region of the tropical rain belt (which will predominantly be a component of the Hadley circulation). Vertical velocity was chosen because of its connection with large-scale atmospheric circulations (e.g., Bony et al. 2004) and its association with rainfall (e.g., Lau and Kim 2015). TCW was chosen to represent changes in the atmospheric water budget because of its sensitivity to changes in large-scale atmospheric circulations and changes in atmospheric thermodynamics (e.g., O’Gorman and Muller 2010). Our results are presented as follows: changes in the spatial patterns of mean climate in section 3a; changes in mean seasonal cycles and mean vertical profiles in section 3b; and, the analysis of 3-hourly data within the rain belt in section 3c, which includes both mean changes and changes in frequency distributions.

2. Climate model, data, and methods

a. Regional climate model configurations

Two RCM configurations, one with parameterized convection (P25) and one with explicit convection permitted (CP4), were run independently for a limited area domain (Stratton et al. 2018). The domain extended from 45°S to 40°N and from 25°W to 56°E to include the whole of Africa and locate the boundaries away from the coast of Africa. Both RCM configurations used the Met Office Unified Model (UM), which is a nonhydrostatic model

with a semi-implicit, semi-Lagrangian dynamical core. Both configurations were based on ENDGame (Even Newer Dynamics for General Atmospheric Modeling of the Environment) dynamics (Wood et al. 2014). Lateral boundary conditions for both configurations were driven by one-way nesting (Davies 2014) in an unnudged global N512 AMIP simulation with 85 vertical levels using the Global Atmosphere/Land 7.0 (GA7/GL7) configuration of the UM (Walters et al. 2019), hereinafter referred to as G25.

1) PARAMETERIZED CONVECTION SIMULATION (P25)

The parameterized convection RCM configuration used a horizontal grid resolution of ~ 25 km latitude and ~ 39 km longitude at the equator, the same as the G25 configuration, and 63 vertical levels up to 41 km. Parameterized convection was based on the Gregory–Rowntree mass flux scheme (Gregory and Rowntree 1990) with several enhancements including, for example, allowance for downdrafts, convective momentum transport, and a closure based on convectively available potential energy (Walters et al. 2017). The prognostic cloud scheme PC2 (Wilson et al. 2008) was used in the P25 configuration (also used in the G25 configuration).

2) CONVECTION-PERMITTING SIMULATION (CP4)

The convection-permitting RCM configuration used a horizontal grid resolution of ~ 4.5 km latitude and longitude at the equator and 80 vertical levels up to 38.5 km. Convection was represented explicitly using the model dynamics although it only partly resolved deep convection on a 4.5-km grid resolution and cannot resolve smaller-scale congestus or shallow convection (Stratton et al. 2018). Previous studies using explicit convection in the UM, however, yielded an improved spatial distribution of rainfall and an improved diurnal cycle compared to TRMM (Birch et al. 2014b) and these improvements were largely a result of explicitly resolving convection rather than finer model resolution (Pearson et al. 2014) and were achieved despite the 4.5-km grid resolution being within the “gray zone” for resolution of convection (Field et al. 2017).

In addition to differences in model resolution and the representation of convection, there are other notable differences between the P25 and CP4 simulations. The large-scale cloud scheme used in CP4 is described by Smith (1990) and has been used in previous convection-permitting versions of the UM. Following Lock et al. (2000), CP4 included stochastic perturbations in the subcloud layer of cumulus-capped boundary layers to improve the triggering of resolved convection.

3) CURRENT CLIMATE SIMULATIONS

The G25 and RCM simulations were forced with sea surface temperatures (SST) derived from the Reynolds dataset of daily high-resolution blended analyses for SST on a regular spatial grid of 0.25° resolution (Reynolds et al. 2007). The G25 simulation was run for years 1988–2010. The current climate (CC) RCM simulations were run for 10 years (1997–2006). Atmospheric greenhouse gas (GHG) concentrations had fixed global values which were updated annually. Aerosol concentrations in the RCMs were based on climatologies from an earlier version of the climate model that used the CLASSIC aerosol scheme (Walters et al. 2019). Aerosols in G25 were interactive and used the U.K. Chemistry and Aerosols (UKCA) scheme. The RCM simulations used GHG concentrations based on those for the G25 simulation and interpolated to their regional model grids. The initial conditions for the RCM atmospheres were taken from the G25 simulation at 1 January 1997. For further details of the G25 and RCM simulations, including tables that list the differences between the RCM simulations, see Stratton et al. (2018).

4) FUTURE CLIMATE SIMULATIONS

The future climate (FC) simulations were run for a period of 10 years using the same setup used for the CC simulations except for changes to the GHG concentrations and the SSTs. The GHG concentrations were taken from year 2100 in projections of representative concentration pathway 8.5 (RCP8.5) (Moss et al. 2010). The SST changes were taken from the climatological average SST change between 1975–2005 and 2085–2115 in a HadGEM2-ES RCP8.5 simulation. These SST changes were calculated for each calendar month, interpolated in space and time, and added to the daily Reynolds SST climatology that was used in the CC simulations. The same aerosol and ozone climatologies were used in the CC and FC simulations.

5) DATA

In our analysis of the RCM simulations, 9 years' worth of data at 3-hourly intervals was used for rainfall, TCW, and vertical velocity. It was computationally too expensive to run these simulations for longer. A strong climate change signal was achieved by using the RCP8.5 climate change scenario and model internal variability was constrained by using observed SSTs in current climate with an increment for climate change. Kendon et al. (2019) found statistically robust changes in extremes and we find statistically robust changes in in the rain belt.

It is important to establish a fair comparison between the CP4 and P25 simulations and ensure that the differences

in vertical motions are consistent with the different treatments for convection. Vertical motions in P25 arise from a resolved large-scale circulation and unresolved subgrid that are closed separately. The subgrid vertical motions are closed locally within each grid cell through the convection parameterization in which subgrid updrafts are balanced by a compensating environmental subsidence. The subgrid vertical motions are derived from the convective mass flux parameterization driven by the vertical profiles of temperature and humidity at the P25 horizontal grid scale (~ 25 km). In contrast, vertical motions arising from convection in CP4 are handled explicitly and are resolved by model physics on the horizontal grid scale (~ 4 km). Vertical velocity at 500 hPa (ω_{500}) from P25 and CP4, consequently, represent circulations at different scales.

Data from the CP4 simulation were, therefore, regrided to the P25 horizontal grid resolution using a conservative remapping function. The scale at which finescale processes are fully resolved in climate model simulations is on the order of four model grid cells or larger (Pielke 2002). To compare the P25 and CP4 simulations on a scale at which convection is expected to be fully resolved, therefore, data for P25 and CP4 were regrided to ~ 150 -km resolution (i.e., 6 times the P25 resolution).

b. Observations

The Tropical Rainfall Measuring Mission (TRMM) Multisatellite Precipitation Analysis 3B42 version 7 rainfall dataset was used for observations of rainfall (Huffman et al. 2010; NASA 2015). The 3B42 rainfall is based on rainfall estimates from multiple satellites combined with bias correction using monthly land surface rain gauge data. Daily mean rainfall was derived from 3-hourly observations of rainfall from 1998 to 2006 (inclusive) on a regular grid resolution of 0.25° . The data were regrided from the TRMM grid to the P25 horizontal grid for ease of comparison against data from the P25 and CP4 simulations.

The CPC morphing technique (CMORPH) produces global satellite precipitation products at a grid resolution of 0.07277° latitude/longitude (8 km at the equator) and a temporal resolution of 30 min (Joyce et al. 2004). Daily mean rainfall data from 1998 to 2006 were derived from the bias-corrected CMORPH product in which satellite-based precipitation estimates have been bias-corrected using station gauge data (Xie et al. 2017). The data were regrided to the P25 horizontal grid for ease of comparison with the regrided TRMM data.

c. Definition of the ascending region of the rain belt

The ascending region of the tropical rain belt was defined as a contiguous region in which zonal daily mean rainfall exceeded 3 mm day^{-1} : a rain rate that, in the P25

and CP4 simulations, enclosed the region of mean ascent in daily mean vertical velocity at 500 hPa and which tracked the seasonal meridional migration of the rain belt. Zonal means were calculated between latitudes 15° and 30°E for each zonal band of grid cells between 25°S and 20°N . This region was chosen to target continental Africa and limit the influence of coastal processes along the west coast of Africa and the influence of the mountainous terrain of East Africa. There remains a gradient in orography, however, from the relatively flat north to the relatively mountainous south of the region. To ensure contiguity in the rain belt, the daily zonal means were calculated as moving averages over a latitude range of nine grid cells and over nine 3-h time steps. Data for winds on pressure levels were available as instantaneous values at 3-h intervals. Hourly mean rainfall rates were, therefore, sampled every 3 h to be consistent with the wind field data.

To mitigate the effects of seasonal changes in the position of the rain belt and differences in its position between P25 and CP4, and between current and future climates, we analyzed only those grid cells that are located within the rain belt. The position of the rain belt was determined daily.

d. Analysis of frequency distributions

The analysis of frequency distributions for rainfall, ω_{500} , and TCW was performed by allocating data counts to data bins. The data were sampled at 3-hourly intervals, from the grid cells located within the ascending region of the tropical rain belt (see section 2c). For rainfall, rainfall events were included for all occurrences of nonzero rainfall and the frequency distribution was expressed as a function of rainfall intensity in uniformly spaced intervals of 1 mm day^{-1} with an additional separate bin for zero rainfall. For the ω_{500} frequency distribution, the data bins were distributed evenly at an interval of 0.01 Pa s^{-1} . For the TCW frequency distribution, the data bins were distributed evenly at an interval of 1 kg m^{-2} . Separate joint frequency tables were produced for the pairwise combinations of rainfall \times ω_{500} and also for rainfall \times TCW. Changes in rainfall, ω_{500} , and TCW between the current and future climates were not normalized for the changes in temperature.

e. Statistical hypothesis tests

A nonparametric sign test was used to test the statistical significance of changes in daily means in Figs. 1 and 2. To remove autocorrelation from the data, the mean seasonal cycle was removed and daily data were averaged into nonoverlapping 10-day periods. A significance level of 5% was used and the tests were applied separately in each grid cell. A two-tailed paired Student's

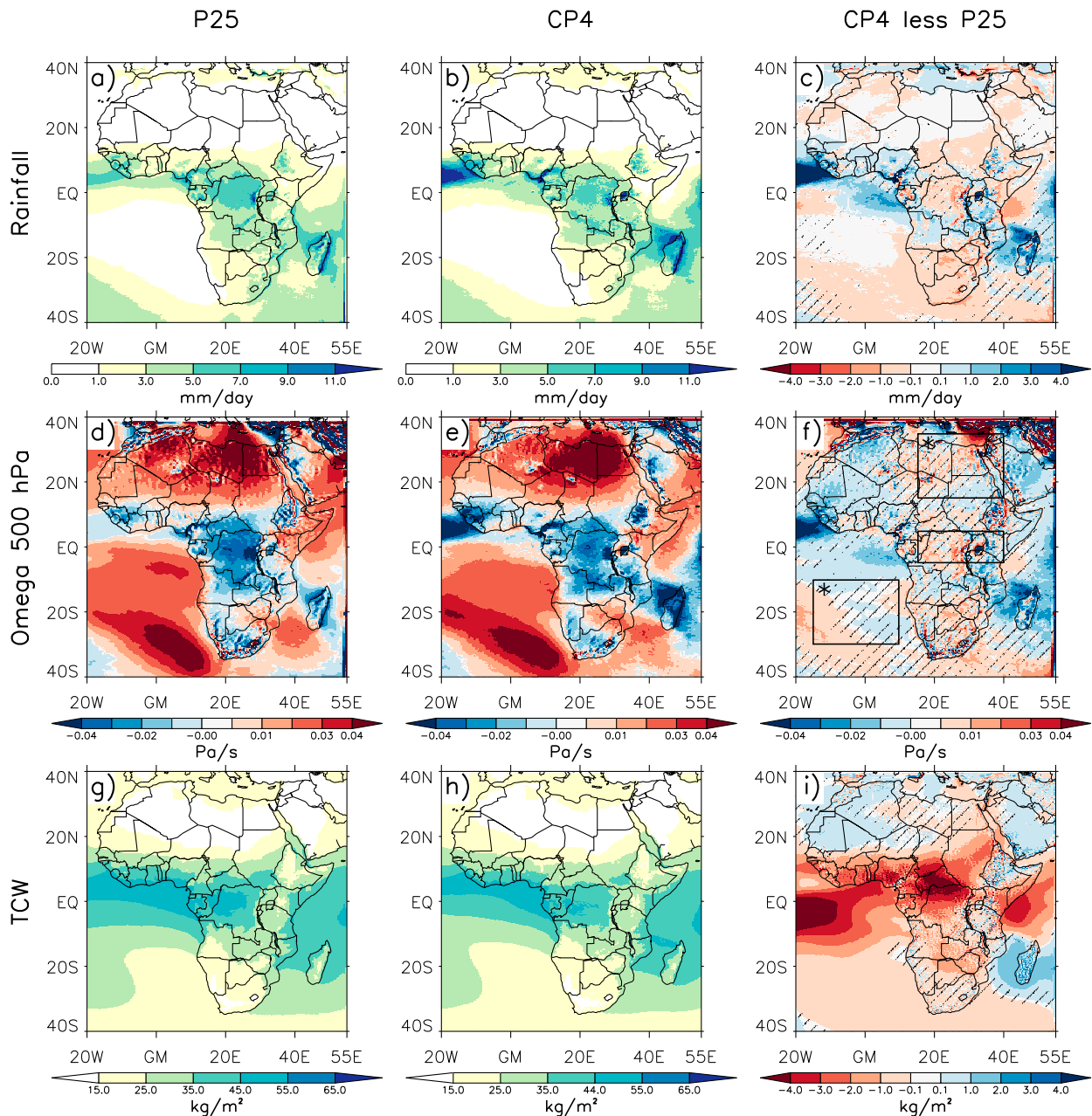


FIG. 1. Annual mean rainfall for (a) P25, (b) CP4, and (c) CP4 less P25. Vertical velocity at 500 hPa for (d) P25, (e) CP4, and (f) CP4 less P25. For vertical velocity, negative values (blue shading) represent mean ascent and positive values (red shading) mean descent. Total column water for (h) P25, (i) CP4, and (j) CP4 less P25. The data are for current climate simulations (1998–2006). Hatching shows regions where the difference between CP4 and P25 is not significant at the 5% significance level. In (f), the three black boxes outline exemplar regions of climatological ascent and subsidence within the Hadley circulation. Boxes where the regional mean change is statistically significant at 5% are marked with a black asterisk.

t test was used to test the statistical significance of changes in monthly means (Fig. 6) and daily means (Figs. 3 and 4). A significance level of 10% was used and the tests were applied separately in each grid cell.

A chi-squared test [see “A test for the continuous distribution of a random variable” in Kanji (2006)]

was used to test the significance of differences between the distributions of rainfall, vertical velocity, and TCW (Figs. 9a, 10a, and 12a). The differences between distributions from CP4 and P25 under the same simulated climate (i.e., current or future climate) were tested. Differences between the current

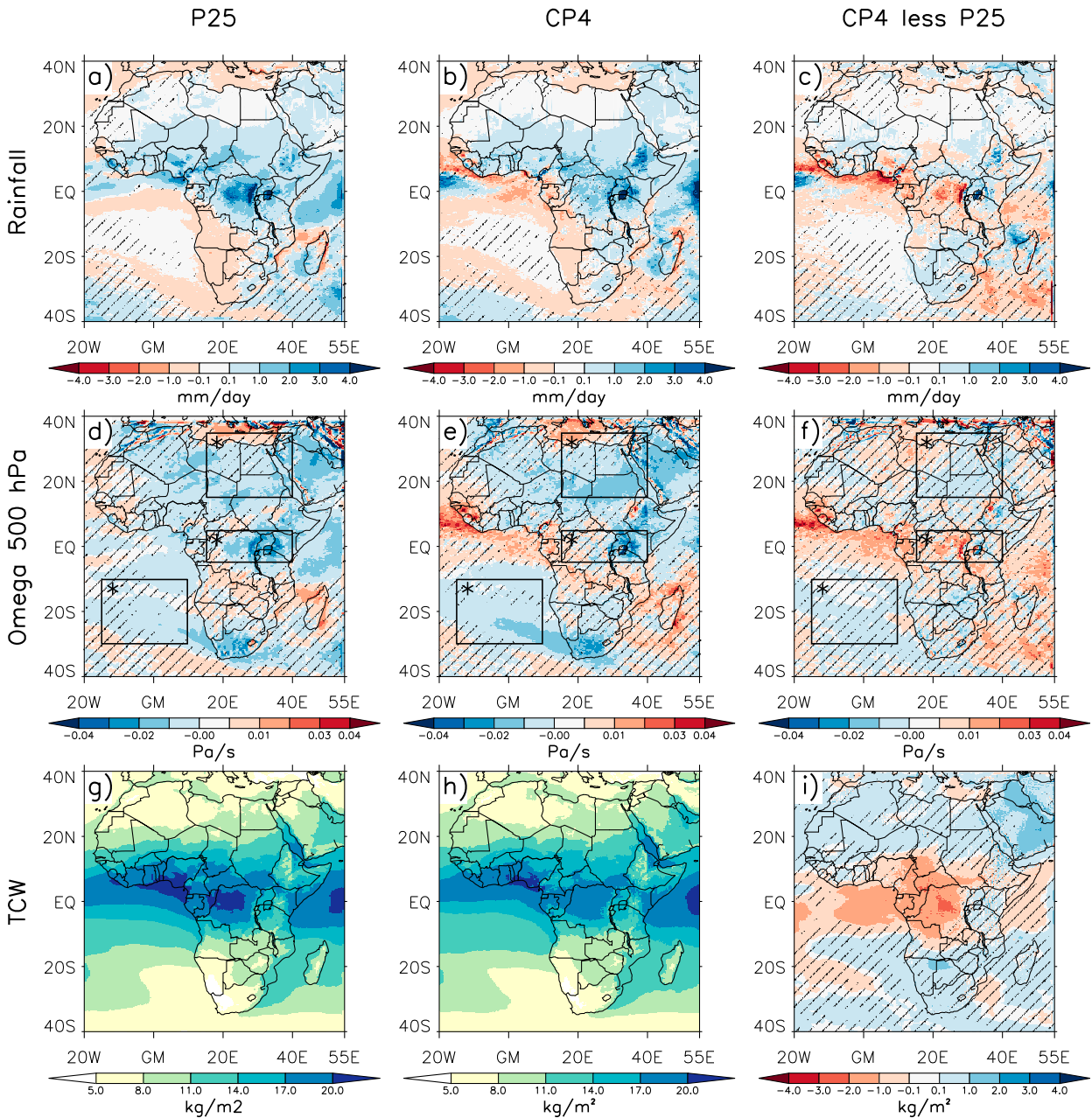


FIG. 2. Change in annual mean rainfall for (a) P25, (b) CP4, and (c) CP4 less P25. Change in vertical velocity at 500 hPa for (d) P25, (e) CP4, and (f) CP4 less P25. For vertical velocity, negative values (blue shading) represent either a strengthening of mean ascent or a weakening of mean descent under climate change. Similarly, positive values (red shading) represent either a weakening of mean ascent or a strengthening of mean descent. Also, changes in total column water are shown for (g) P25, (h) CP4, and (i) CP4 less P25. The changes are between the current and future climates simulations. Note that (c), (f), and (i) show the difference in climate change between the CP4 and P25 simulations. Hatching shows regions where the difference between CP4 and P25 is not significant at the 5% significance level. In (d), (e), and (f), the three black boxes outline exemplar regions of climatological ascent and subsidence within the Hadley circulation. Boxes where the regional mean change is statistically significant at 5% are marked with a black asterisk.

and future climate simulations from the respective models were also tested. A significance level of 1% was used. The same chi-squared test and significance level was used to test the significance of differences

between the current and future climate simulations for the distributions of rainfall contribution by vertical velocity and TCW data bins (Figs. 11c,d and 12b) in P25 and CP4.

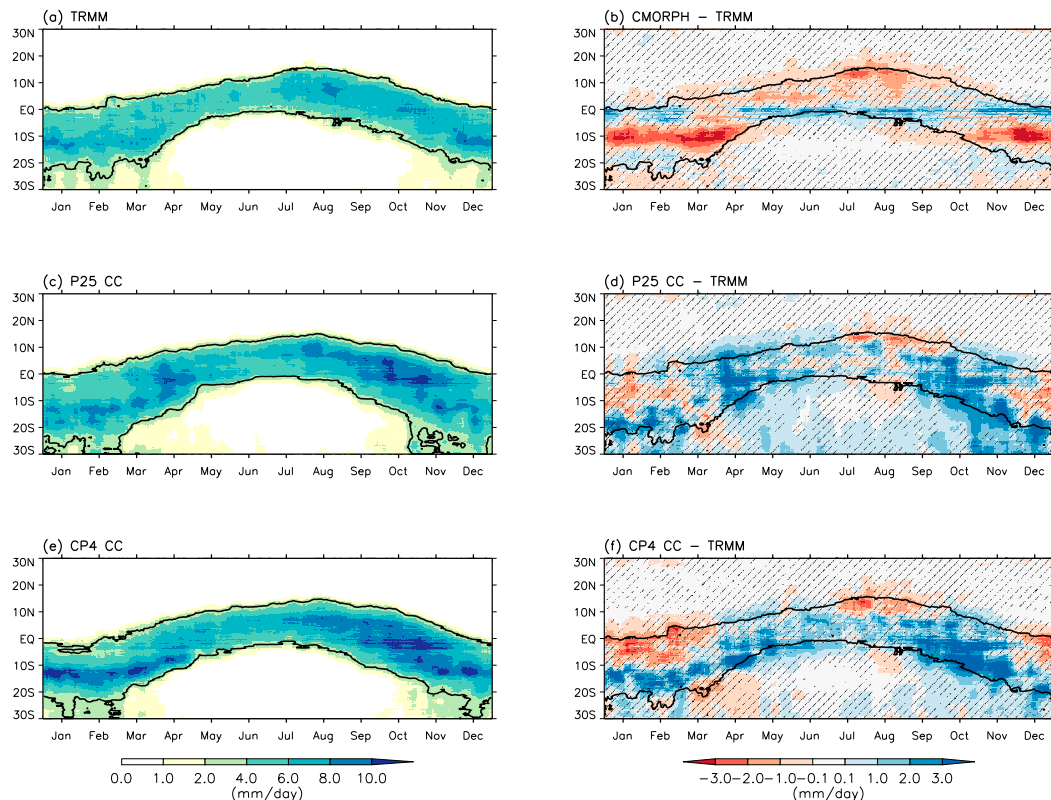


FIG. 3. The seasonal cycle for daily zonal mean rainfall averaged over longitudes from 15° to 30°E and smoothed using a 9-day moving average: (a) TRMM, (b) difference between CMORPH and TRMM, (c) P25 current climate, (d) CP4 current climate, (e) the difference between TRMM and P25 current climate, and (f) the difference between CP4 current climate and TRMM. The used data are 9 years of daily mean data from 1998 to 2006. Contours for rainfall at 3 mm day^{−1} rainfall are overlaid in black. Hatching shows regions where the difference in means is not significant at the 10% significance level.

A nonparametric difference sign test [see “The difference sign test for randomness in a sample” in Kanji (2006)] was used to test the statistical significance of differences between the climate changes of P25 and CP4 for rainfall, vertical velocity, and TCW distributions (Figs. 9d, 10d, and 12a). A significance level of 1% was used. The chi-squared test was not applied because these changes involved both positive and negative data values: The chi-squared test requires data to be positive (i.e., resemble counts data).

3. Results and discussion

In this section, results for time-averaged mean climate are presented in sections 3a and 3b. Changes in the annual mean climatology are presented in section 3a (Figs. 1 and 2). Changes in the seasonal cycle are presented in section 3b and are based on daily means (Figs. 3 and 4) and monthly means (Figs. 5 and 6). Changes in annual mean vertical profiles are also presented in section 3b (Fig. 7). These

results provide context for the subsequent analysis of changes in the tropical rain belt itself. The analysis of changes in the frequency distributions of 3-hourly data within the rain belt (defined in section 2c) are presented in section 3c.

a. Pan-Africa rainfall, ω_{500} , and TCW

1) CURRENT CLIMATE (ANNUAL MEANS)

Over the whole of Africa the spatial patterns of annual mean rainfall, ω_{500} , and TCW are similar between P25 and CP4 (Fig. 1) with a Pearson product-moment correlation coefficient of +0.92 for rainfall over land. Around the equator, CP4 has less rainfall, weaker vertical motion, and less TCW over the Congo basin and the Horn of Africa, with more rainfall over the East African highlands [as described by Finney et al. (2019)]. Immediately south of this, there is more rain in CP4, especially over Madagascar, and less rain in CP4 farther south in the more subsidence-dominated southern Africa (Hart et al. 2018). To the north,

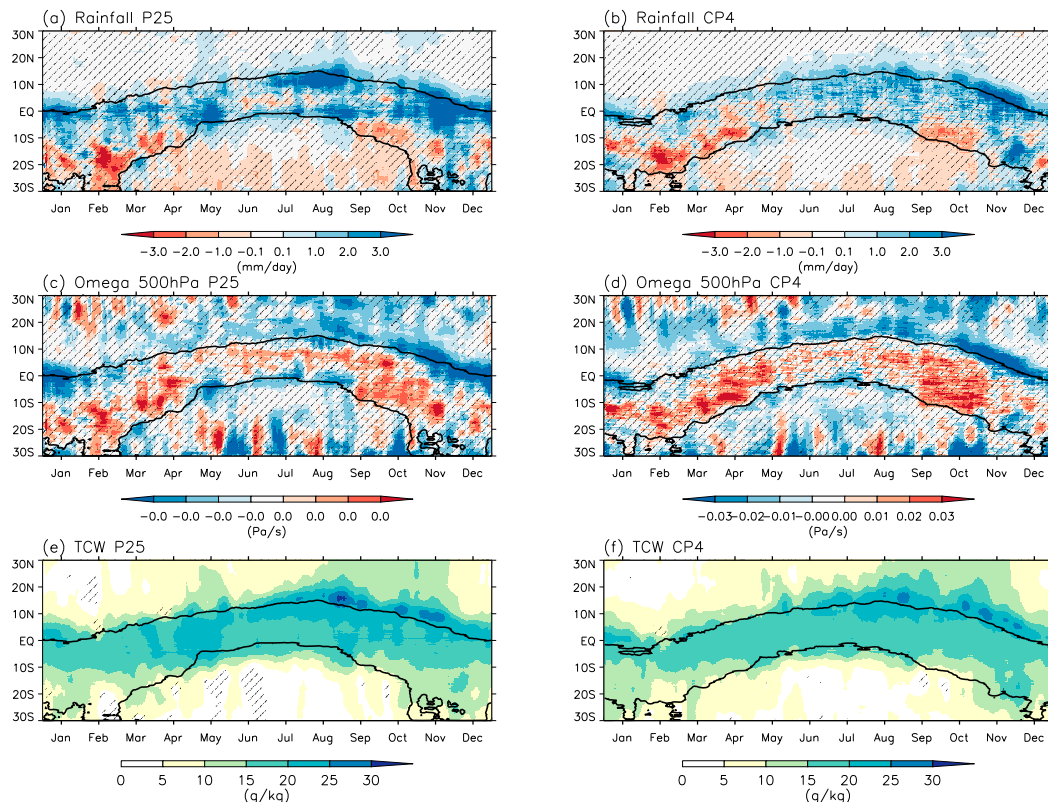


FIG. 4. Differences between future and current climate zonal daily means averaged over longitudes 15° – 30° E for (a) P25 rainfall, (b) CP4 rainfall, (c) P25 vertical velocity at 500 hPa, (d) CP4 vertical velocity at 500 hPa, (e) P25 TCW, and (f) CP4 TCW. For omega, negative values (blue shading) represent either a strengthening of mean ascent or a weakening of mean descent under climate change. Similarly, positive values (red shading) represent either a weakening of mean ascent or a strengthening of mean descent. Contours for rainfall at 3 mm day^{-1} rainfall are overlaid in black. Hatching shows regions where the difference in means is not significant at the 10% significance level.

CP4 has more rain over the Gulf of Guinea and southern West Africa, with more ascent, but less TCW. Although more rain in P25 or CP4 tends to correspond to both stronger ascent and more TCW, this is not always the case. The spatial distribution of large-scale vertical circulation is similar in P25 and CP4 (Figs. 1d,e) although the vertical velocities differ with, for example, stronger rates of subsidence in CP4 compared to P25 over northeast Africa and the southeast Atlantic Ocean (Fig. 1f).

2) CLIMATE CHANGE (ANNUAL MEANS)

Under climate change, annual mean rainfall tends to increase in tropical regions, but not in subtropical southwest Africa (Figs. 2a,b). Climate change in rainfall is correlated between the RCM configurations, with Pearson product-moment correlation coefficients of +0.60 and +0.77 (on 25- and 150-km grid scales, respectively). This shows that although the changes are correlated, there is still much variation in the spatial pattern of change and therefore the representation of convection remains a source of uncertainty. There is a slowdown in mean subsidence with

weaker subsidence over the Sahara Desert, the Arabian Peninsula, southern Africa, and the southeast Atlantic Ocean (Figs. 2d,e). Ascent within the very core of the rain belt over central Africa (5°S – 5°N) is strengthened in future climate in both P25 and CP4 (Figs. 2d,e). P25 and CP4 both show an increase in TCW (Figs. 2g,h).

Under climate change, CP4 has a relative slowdown in vertical circulations compared to P25. CP4 has a greater slowdown of climatological subsidence in many regions in the subtropics (Fig. 2f). Around Lake Victoria (East Africa) ascent gets stronger in both CP4 and P25, although less so in CP4 (Fig. 2f). Over central Africa, to the west of Lake Victoria, ascent in CP4 typically either weakens by more, or strengthens less, than in P25. TCW increases less about the equator in CP4 than in P25, broadly where climatological ascent prevails, and increases more in CP4 in the subtropics where climatological subsidence prevails (Fig. 2i). Changes in mean rainfall across Africa are relatively weakly correlated with changes in mean ω_{500} , with Pearson product-moment correlation coefficients of -0.21 and -0.38 in

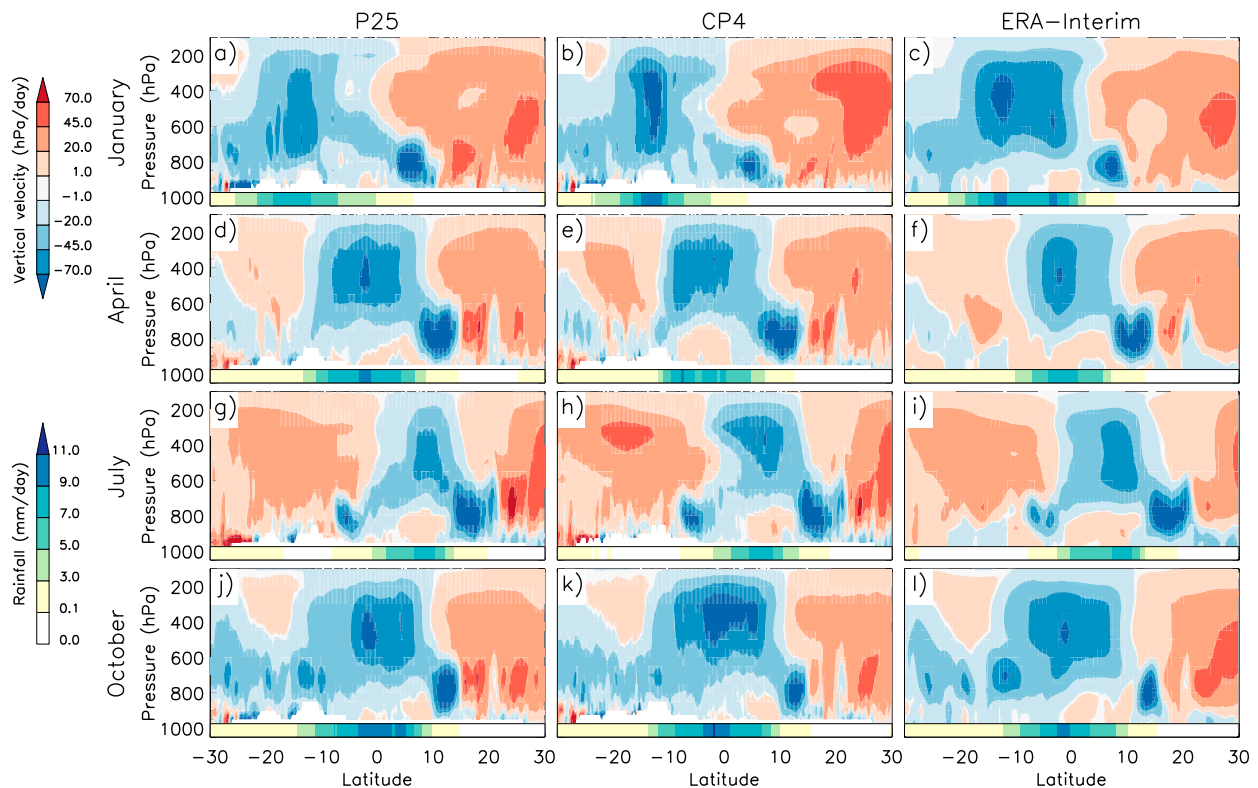


FIG. 5. Vertical cross sections of monthly mean vertical pressure velocity (colored contours) averaged over the longitudes from 15° to 30° E in the months of (a)–(c) January, (d)–(f) April, (g)–(i) July, and (j)–(l) October. The current climate simulations of (left) P25 and (center) CP4, and (right) ERA-Interim. Blue shading represents mean ascent and red shading mean subsidence. Zonal mean precipitation is shown in the horizontal color bar at the bottom of each cross-section plot for P25, CP4, and ERA-Interim, from left to right, respectively.

P25 and CP4, respectively. These differences show the response of rainfall to forcing by increased greenhouse gases and warming of SSTs. We note, however, that future changes in aerosols, not directly captured in the RCM simulations, will also affect future rainfall patterns (Scannell et al. 2019; Seth et al. 2019).

The climate changes in rainfall and TCW are statistically significant in many places (Figs. 2a,b,g,h). Statistically significant differences between the climate changes of P25 and CP4 for rainfall are widespread and may be limited in some regions by the relatively short length of the time series (9 years). The climate change in TCW differs between P25 and CP4 over central Africa. While differences between the climate changes of P25 and CP4 for ω_{500} are not statistically significant in many grid cells, regional changes are more robust with significant changes occurring in both regions of mean subsidence and mean ascent (Fig. 2f).

b. The tropical rain belt rainfall, ω_{500} , and TCW

1) SEASONAL CYCLE (DAILY MEANS)

The tropical rain belts in P25 and CP4 capture the prominent features of the annual cycle of rainfall over

tropical Africa. In TRMM observations (Fig. 3a): the rain belt is at its most northerly position in late July/early August, is widest in February and narrowest in May, and has its most intense rainfall during July to December. Rainfall in P25 (Fig. 3c) and CP4 (Fig. 3e) follows a similar annual cycle. The rainfall in P25 and CP4 is frequently greater than TRMM within the rain belt (Figs. 3d,f). Regional biases will be due, in part, to biases in the positioning of the rain belt as well as biases in local rainfall frequency, intensity, and duration. Notably, during December–February and July–August the most intense rainfall in P25 and CP4 is located farther south than in TRMM and P25 has larger biases than CP4 south of the rain belt all year round. Uncertainty in the position and intensity of the rain belt within TRMM observations is demonstrated by comparison with CMORPH observations (Fig. 3b). CMORPH is wetter than TRMM along the equator and drier toward the poleward margins of the rain belt. P25 and CP4 are largely outside the range of the observations, being wetter than TRMM and CMORPH, although more than 9 years of data would be necessary to establish statistical significance throughout the rain belt.

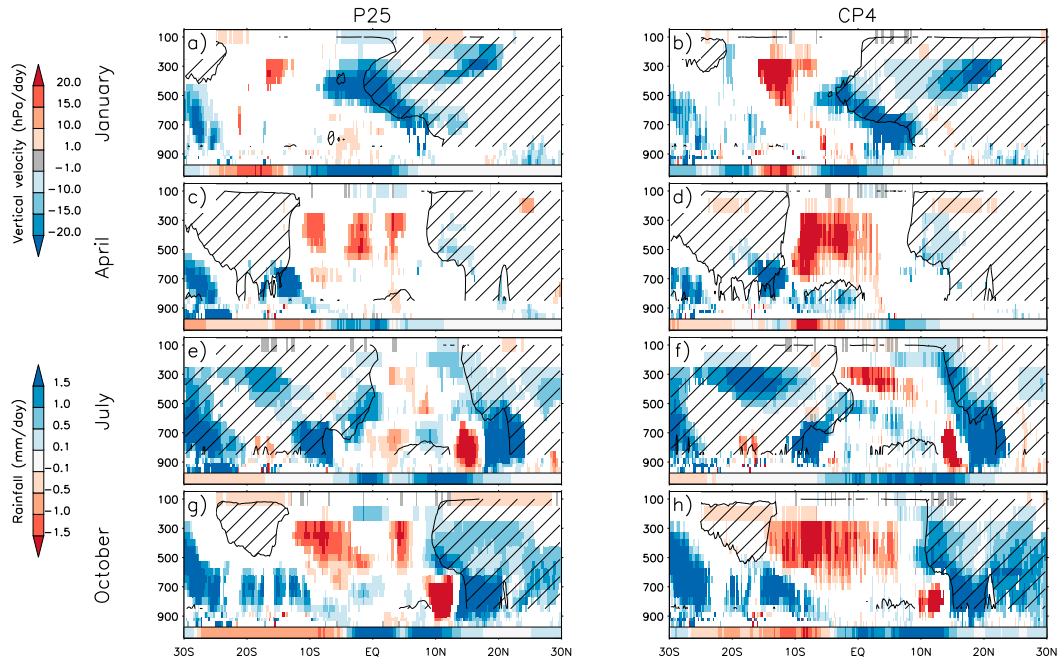


FIG. 6. Vertical cross sections of the change in monthly mean vertical pressure velocity between the future and current climate simulations averaged over longitudes from 15° to 30° E (colored contours). The months of January, April, July, and October are shown by row and the P25 and CP4 simulations by column. Blue shading represents either an intensification of upward motion or a weakening of downward motion. Equivalently, red shading represents either an intensification of mean subsidence or a weakening of mean ascent. Regions where the difference in means is not significant at the 10% significance level are shaded white. Hatching shows the regions of mean subsidence in the current climate simulations. The change in zonal mean precipitation is shown in the horizontal color bar at the bottom of each cross-section plot.

Zonal mean rainfall increases in future climate and there is a northward shift in the rain belt (Figs. 4a,b). A northward shift has previously been noted in global models, and linked to changes in the Saharan heat low (Dunning et al. 2018). The shift in rainfall is similar in P25 and CP4 (Figs. 4a,b), which is accompanied by a northward shift in ω_{500} (Figs. 4c,d) and TCW (Figs. 4e,f). Zonal mean ω_{500} within the 3 mm day $^{-1}$ contours of the tropical rain belt is predominantly shaded red, which represents a net weakening of ascent. Zonal mean TCW increases in the future climates of both P25 and CP4, induced by the increase in air temperature, but also responding to changing circulation. The increases in TCW are greatest along the northern margin of the rain belt and are accompanied by increases in rainfall in the same locations. The increases in rainfall are widespread and particularly prevalent on the northern side of the rain belt over, the Congo basin in November–January, the Central African Republic and South Sudan in October, and as far north as Chad and Sudan in July–August. The July–August increase is less pronounced in CP4 compared to P25 despite its more pronounced ω_{500} change, but consistent with the

greater TCW change in P25. This reveals differences between P25 and CP4 in the interactions between changes in ω_{500} and TCW and their influence on rainfall change. On the southern side of the rain belt, rainfall decreases over Angola and Zambia in January–April (with some small but potentially significant differences between P25 and CP4) and over the Congo basin ($\sim 10^{\circ}$ S) in September–October. The most conspicuous difference between the P25 and CP4 simulations occurs over the Congo basin (approximately at the equator) where rainfall and TCW are enhanced more strongly in P25, most notably in May.

2) VERTICAL STRUCTURE (MONTHLY MEANS)

The vertical structure and seasonal migration of the rain belt in ERA-Interim, which while using parameterized convection is constrained by data assimilation, is shown in Fig. 5 (right-hand column). The core of the rain belt is defined by the collocation of heavy monthly mean rainfall beneath strong upward vertical motion in the midtroposphere (e.g., at 500 hPa) and weaker vertical motion in the lower troposphere that frequently involves subsidence (e.g., at 850 hPa). The rain belt is

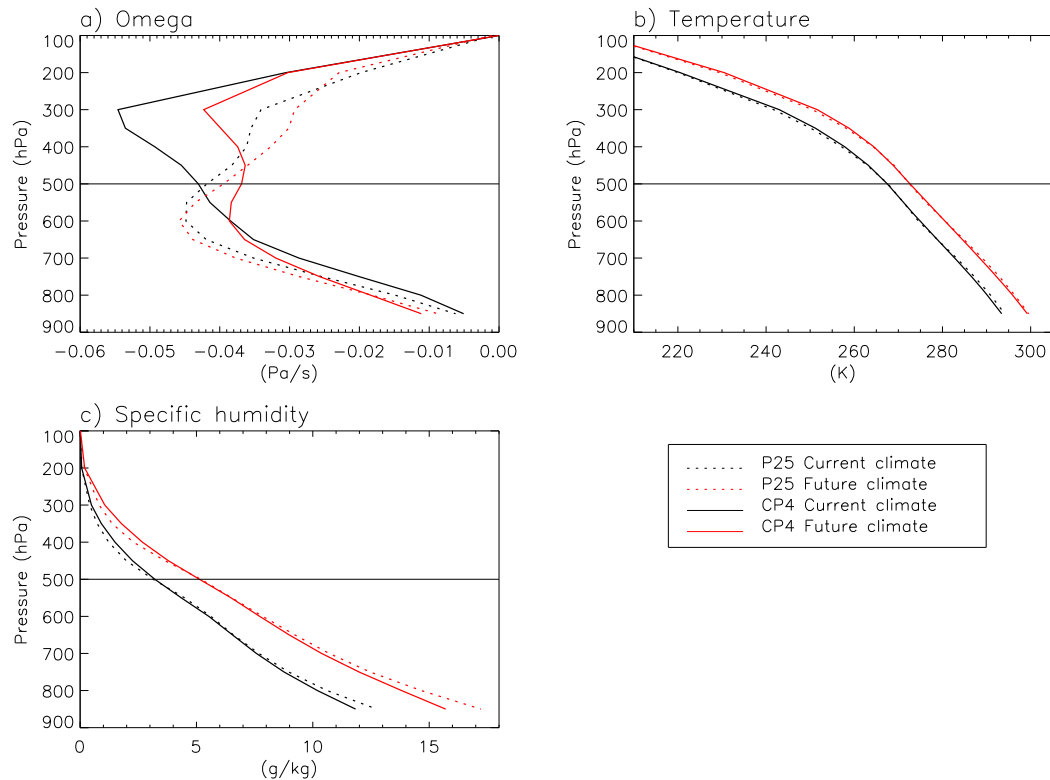


FIG. 7. Mean vertical profile of (a) vertical velocity, (b) temperature, and (c) specific humidity. The vertical profiles are averaged over the region 15° – 30° E and over latitudes within 20° S– 15° N where smoothed monthly mean rainfall exceeds 3 mm day^{-1} . The data used for this figure are from years when there are no missing pressure level data (i.e., the last 6 years of each simulation). For vertical velocity, negative values represent mean ascent.

topped by divergent winds at 200 hPa and the tropical easterly jet. The core of the rain belt is bounded to the north and south by the subsiding branches of the Hadley circulation. The rain belt migrates north–south following the latitude of maximum insolation with a lag of approximately one month, which is consistent with satellite observations of migrations in deep convective clouds (Waliser and Gautier 1993) and the description of the migration of the tropical rain belt over Africa in McGregor and Nieuwolt (1998) and Hart et al. (2019). The rain belt is preceded in its migration by a region of shallow ascent that yields moderate rainfall (~ 1 – 3 mm day^{-1}) and is not collocated with the core rain belt (Nicholson 2018). The shallow ascent has low-level convergence of trade winds on its poleward side, the intertropical discontinuity (ITD), and is topped by midlevel subsidence on its equatorward side and the African easterly jets (AEJs) (not shown). The shallow ascent itself is perennial to the north of the rain belt and seasonal to the south where its separation from the rain belt core is apparent in May to September (Fig. 5, July).

The vertical structure and seasonal cycle of the tropical circulation in the P25 and CP4 simulations (Fig. 5, center and left-hand columns) closely match ERA-

Interim. Most importantly for this study, both simulations capture the collocation of the intense rainfall beneath strong ascent in the midtroposphere ($\sim 500 \text{ hPa}$). CP4 gives greater winter hemisphere upper-level descent than P25, as noted by Hart et al. (2018), although this descent is too strong and narrow compared with ERA-Interim.

Under climate change (Fig. 6), the ascending branch of the tropical circulation widens and vertical motions weaken. The widening of the ascending circulation is most apparent to the north in July and October, shown by the blue shading at low levels to midlevels spanning the boundary between mean ascent and mean subsidence in current climate. Weaker ascent in the rain belt is shown by the red shading at midlevels. This is accompanied by widespread weaker subsidence to the north of the rain belt (i.e., in the subsiding branch of the tropical circulation), shown by the blue shading at mid- and upper levels in the hatched regions.

Vertical profiles of annual mean resolved vertical velocity, temperature, and humidity within the rain belt region are shown in Fig. 7. Resolved vertical motion is deeper in CP4 than in P25 with a peak vertical velocity

higher in the atmosphere at ~ 300 hPa in CP4 compared to ~ 550 hPa in P25. The effect of deeper vertical motion in CP4 is apparent in the vertical profiles of temperature and humidity. The lapse rate is weaker in CP4 than in P25 and, similarly, the vertical gradient in specific humidity is weaker in CP4, suggesting that the net upward vertical transport of heat and moisture is stronger in CP4. Although vertical motion is deeper in CP4, mean vertical velocities at 500 hPa and below are weaker than in P25. Under climate warming, mean upward vertical velocity between 250 and ~ 600 hPa is weaker in both P25 and CP4, while increases above are consistent with a deepening troposphere. The greatest reductions occur at ~ 300 hPa and are much greater in CP4 than P25. In contrast, upward vertical velocity is stronger in the lower troposphere (800–700 hPa) in both simulations. The changes in vertical velocity profile with climate change were accompanied by an increase in temperature and an increase in specific humidity throughout the atmospheric column, with greater warming above 350 hPa in P25, and greater moistening at these levels in CP4, showing a greater increase in transport of water vapor to high altitudes under climate change by more vigorous convection in CP4.

c. Distributions of rainfall, ω_{500} , and TCW within the rain belt

In sections 3a and 3b we have shown that there are marked differences in changes to mean climate between P25 and CP4. To gain insight into these differences, in this section we describe the frequency distributions of 3-hourly rainfall and ω_{500} and then investigate their relationships and changes under climate change. To avoid obscuring subtleties in the relationships, the results below use data at the 25-km grid scale and at 3-hourly intervals (section 2d) and use data from grid cells identified as within the rain belt (defined separately within each simulation and in each climate) according to the definition in section 2c.

The simulations of mean rainfall, ω_{500} , and TCW in current climate are similar in P25 and CP4 differing by 3%, 2%, and 2% respectively (Figs. 8a,c,d). As expected from their differing representations of convection, the character of the rainfall is very different between P25 and CP4: rainfall occurs less frequently in CP4 compared to P25 (Fig. 8b).

There are more marked differences, however, between the simulations of future climate. The increases in TCW are similar at 40.9% in CP4 and 43.1% in P25 (Fig. 8d), which is consistent with slightly greater warming in P25 than CP4 (not shown) and similar small changes in relative humidity (not shown). Rainfall, however, increased by 5.5% and rain frequency by -29.7% in CP4 compared to changes of 14.1% and -13.1% respectively in P25

(Figs. 8a,b) and ω_{500} decreased by 17.3% in CP4 compared to 9.8% in P25 (Fig. 8c).

The increase in mean rainfall in both P25 and CP4 is consistent with the range of increases in rainfall for the tropical rain belt over Africa projected by the CMIP5 models (Christensen et al. 2013). The difference in mean rainfall change between resolved and parameterized convection in the central African transect is large. Kooperman et al. (2016) also found that simulations using resolved convection projected smaller mean changes in rainfall over land than simulations with parameterized convection using the same model. Our results highlight the magnitude of uncertainty in projections of future rainfall over tropical Africa that arises from convection parameterization, a region where there is not even consensus for the sign of the rainfall change (Christensen et al. 2013).

1) RAINFALL FREQUENCY DISTRIBUTION

Relatively light rainfall is more frequent in P25 than in CP4 (Fig. 9a) whereas relatively heavy rainfall is more frequent in CP4 and is most clearly shown in the distributions of rainfall contribution (Fig. 9b) and cumulative rainfall contribution (Fig. 9c). In the current climate simulations, the P25 simulation has a greater cumulative contribution up to ~ 200 mm day $^{-1}$ (on the 25-km grid) because of the more frequent occurrence of lighter rainfall (Fig. 9c). CP4 has greater mean rainfall in the current climate simulation because of the more frequent occurrence of heavier rainfall, particularly above ~ 200 mm day $^{-1}$ (Fig. 9c). The contribution was calculated as the sum of the rainfall in each data bin divided by the total number of data points in all data bins. The sum of the contributions over all data bins, therefore, equals the mean rainfall and is represented graphically as the area under each contribution curve. Differences in the frequency distributions of rainfall of P25 and CP4 are consistent with previous comparisons of PCMs and CPMs (Prein et al. 2015). Kooperman et al. (2016), in a study comparing simulations using parameterized convection against superparameterization, and Kendon et al. (2019) in a study using the simulations described here, show that heavy rain rates under climate change are intensified when convection is resolved.

Under climate change, both P25 and CP4 project an increase in heavy rainfall (exceeding ~ 175 mm day $^{-1}$ on the 25-km grid) and both project a decrease in the lightest rainfall (Fig. 9d). CP4, however, also projects a marked decrease in rainfall between 50 and 175 mm day $^{-1}$ intensity contributing to the weaker increase in mean rainfall in CP4 compared to P25 (Figs. 9b,d). These differences remain after regridding to a coarser 150-km grid resolution (not shown), indicating that they are robust to

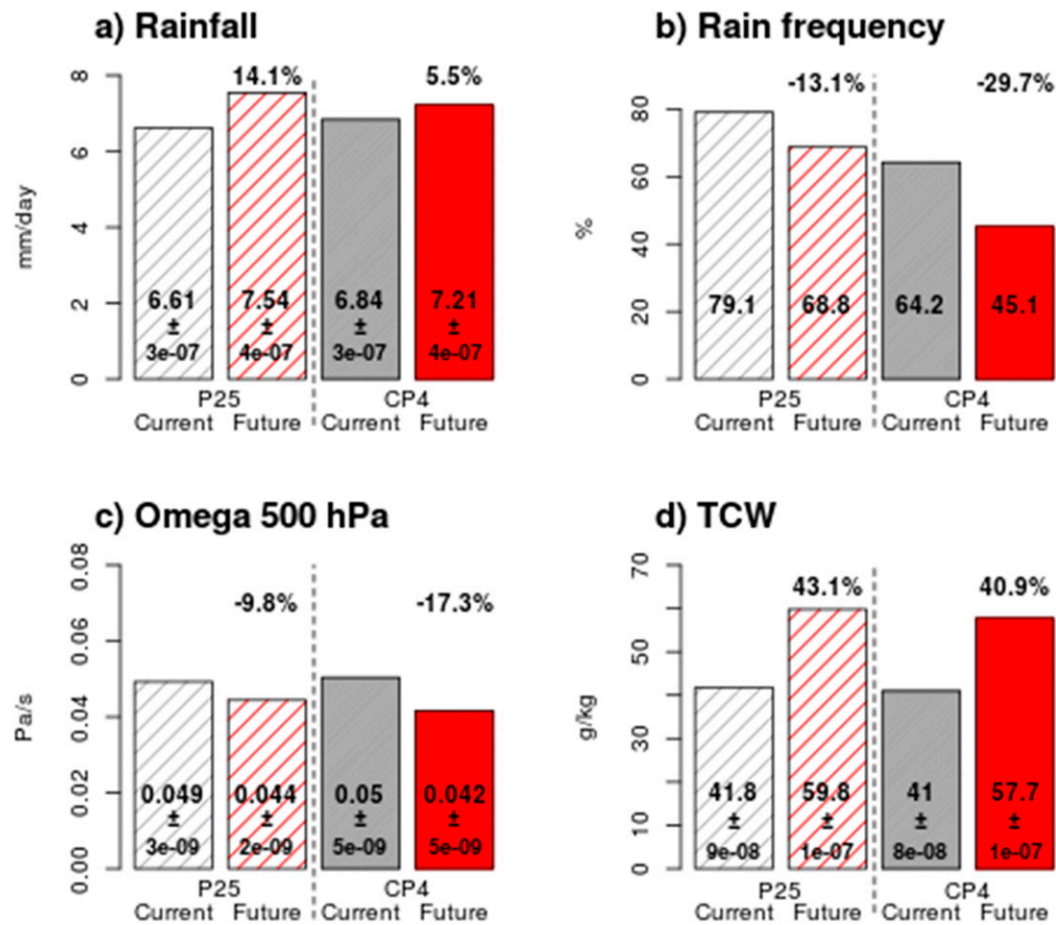


FIG. 8. Annual mean (a) rainfall, (b) rain frequency, (c) vertical velocity at 500 hPa (ω_{500}), and (d) total column water (TCW). The means are for the rain belt region as defined in section 2d. Also shown are the percentage changes from current to future climate for P25 and CP4. For vertical velocity, mean ascent is represented by positive values.

changes in spatial resolution and related to the different representations of convection in P25 and CP4.

2) ω_{500} FREQUENCY DISTRIBUTION

Relatively weak vertical motions of about 0 Pa s^{-1} are more frequent in P25 than in CP4 (Fig. 10a). Relatively intense ascending and descending motions are more frequent in CP4 and contribute to a larger variance for the ω_{500} distribution in CP4 (2.19) than in P25 (0.09). The distributions of ω_{500} in P25 and CP4 are negatively skewed, which highlights that the tails of the distributions are longer on the ascending side, although skewness is greater in the CP4 distribution with skewness of -15.2 compared to -4.2 in P25. Differences in the tails of the distributions are more clearly shown in the distributions of ω_{500} contribution (Fig. 10b) and cumulative ω_{500} contribution (Fig. 10c). In the current climate simulations, the CP4 simulation has a greater

cumulative contribution to net ω_{500} at all but the weakest of vertical motions. Differences in the distribution of rainfall and ω_{500} arising in CP4 are consistent with an improved physical representation of the rain belt region which comprises tall, narrow towers of strong convection separated by larger-scale regions of subsidence (Riehl and Malkus 1958).

Under climate change, P25 projects a modest increase in updrafts at $\sim 2 \text{ Pa s}^{-1}$ (on the 25-km grid) and a weaker mean ω_{500} largely due to fewer weak updrafts (Fig. 10d). CP4 projects more marked changes in its distribution: an increase in frequency of intense updrafts (from ~ -10 to $\sim 3 \text{ Pa s}^{-1}$ on the 25-km grid); a decrease in frequency of relatively weak updrafts (weaker than -3 Pa s^{-1}) that is large enough both to offset the contribution to mean ω_{500} from the changes in intense updrafts and to account for the weakening of the mean ω_{500} ; and an increase in relatively intense downdrafts (Fig. 10d). These differences

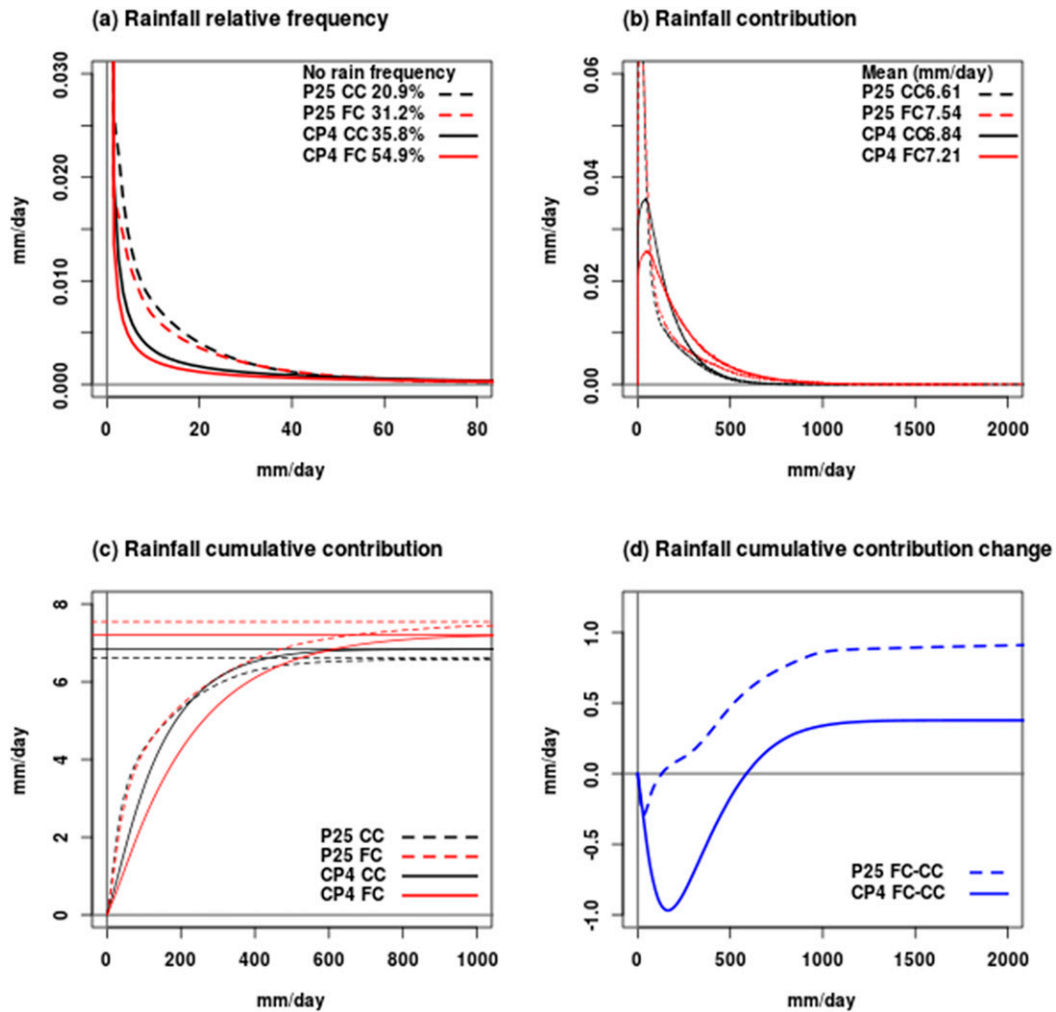


FIG. 9. (a) Frequency distribution for rainfall within the tropical rain belt in the P25 and CP4 current and future climate simulations. (b) The distribution of contribution to mean rainfall. The area under each curve integrates to the mean rainfall shown in the top right of the plot. (c) The cumulative distribution of contribution to mean rainfall starting from zero on the left-hand side and summing to the mean value on the right-hand side. The mean rainfall is represented by the horizontal lines. (d) The distribution of the difference in contribution between the simulations of future and current climate. Changes in the distributions of P25 and CP4 under climate change and the differences between these changes are statistically significant at the 1% level. Key: current climate (black), future climate (red), climate change (blue), P25 (dashed lines), and CP4 (solid lines).

between P25 and CP4 remain after regridding to a coarser 150-km grid resolution (not shown). It is also noteworthy that the changes in ω_{500} in CP4 resemble the observed changes in thunderstorms over the Congo basin from 1982 to 2016 where the trends are toward more intense, deeper storms but with weaker rates of mean ascent at all levels (Raghavendra et al. 2018). The greater decrease in frequency of weak ascent in CP4 (Fig. 10d), together with the decreases in rain frequency and light rainfall, is consistent with a shift to a more stable atmosphere likely in future climate (Chou et al. 2012). The marked shift from weak to strong updrafts in CP4 compared to P25 and the greater slowdown in mean ascent raises important questions for the “deep-tropics

squeeze” of Lau and Kim (2015). Are the CMIP5 models underestimating the slowdown in mean tropical circulation while, at the same time, underestimating the frequency of intense rates of ascent in tropical storms?

To show more clearly the role of convection in vertical motion, we calculated the net cumulative contribution for ω_{500} by offsetting upward and downward vertical velocities with the same absolute magnitude (Figs. 10e,f). For relatively weak vertical motions, this effectively cancels out opposing motions likely due to gravity waves. For the P25 simulation of current climate (Fig. 10e), the net vertical motion is upward at almost all vertical velocities. Net ascent in the velocity range $0-1 \text{ Pa s}^{-1}$ accounted for more than 50% of the contribution to net motion and $\sim 95\%$ of the

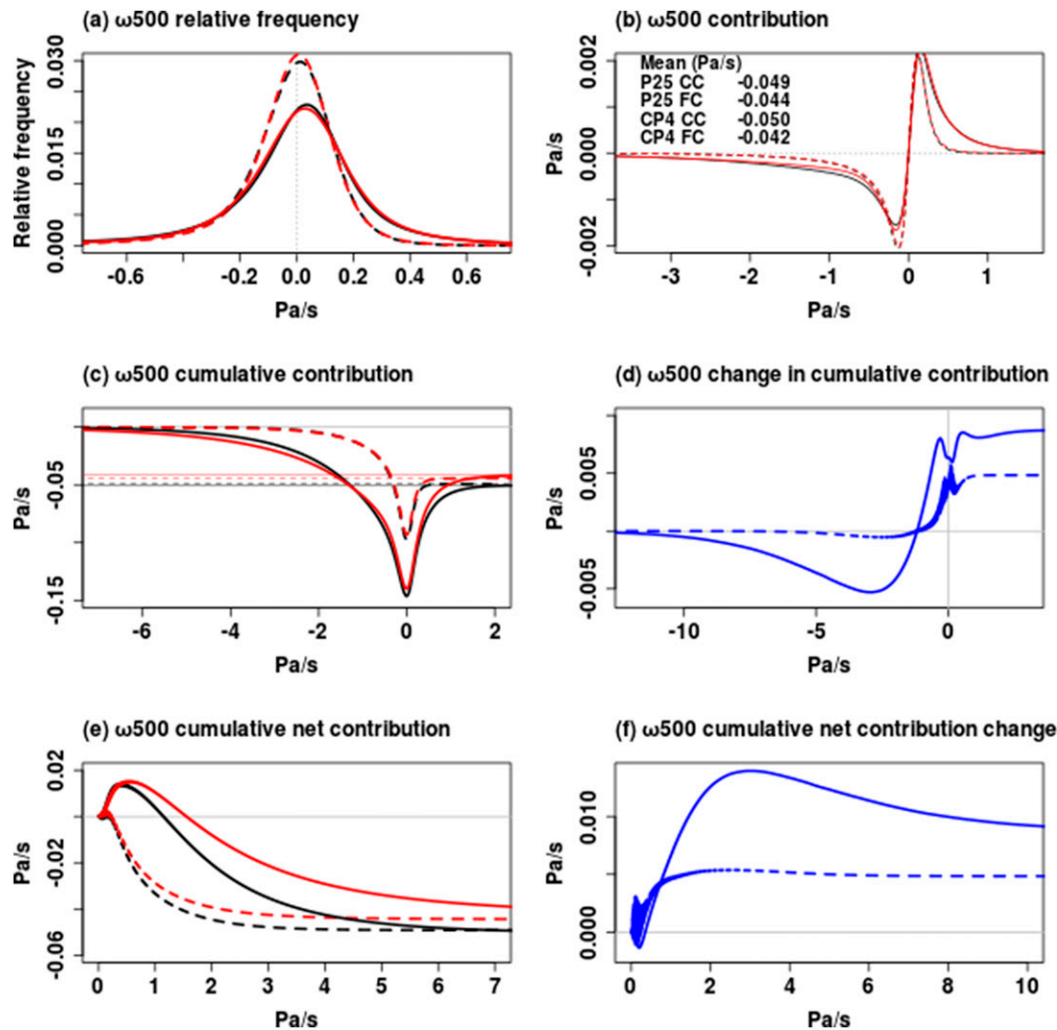


FIG. 10. (a) Frequency distribution for vertical velocity at 500 hPa (ω_{500}). (b) The distribution of contribution to mean ω_{500} . The area under each curve integrates to the mean vertical velocity shown in the top left of the plot. (c) The cumulative distribution of contribution for ω_{500} starting from zero on the left and summing to the mean value on the right. Mean ω_{500} is represented by the horizontal lines. (d) The difference in contribution between the simulations of future and current climate. (e) The cumulative net contribution to mean ω_{500} . (f) The difference in net contribution between the simulations of future and current climate. Changes in the distributions of P25 and CP4 under climate change and the differences between these changes are statistically significant at the 1% level. Key: current climate (black), future climate (red), climate change (blue), P25 (dashed lines), and CP4 (solid lines). In (a)–(d) negative values for ω_{500} represent ascent and positive values descent.

contribution to net motion was accounted for by net ascent weaker than 2.8 Pa s^{-1} (on the 25-km grid). In contrast, for CP4 the net downward motion predominated in the velocity range from 0 to $\sim 0.5 \text{ Pa s}^{-1}$. Net ascent dominated the contribution to mean net motion at greater vertical velocities with $\sim 95\%$ of the cumulative contribution only achieved by 6 Pa s^{-1} . Changes in the cumulative net contributions of ω_{500} also show that the differences between P25 and CP4 persist when opposing vertical motions are offset against one another (Fig. 10f). For P25, the majority of the weakening in net ascent

occurs at velocities less than $\sim 1 \text{ Pa s}^{-1}$. In contrast, for CP4, weaker net ascent occurs up to $\sim 3 \text{ Pa s}^{-1}$ vertical velocity and a greater contribution to the net ascent is apparent from rates of ascent in excess of $\sim 3 \text{ Pa s}^{-1}$. These changes in net cumulative contribution persist after smoothing to a 150-km grid resolution (not shown).

3) THE RELATIONSHIP BETWEEN RAINFALL AND VERTICAL VELOCITY

In both P25 and CP4, more intense vertical motion is associated with more intense rainfall. This is shown by

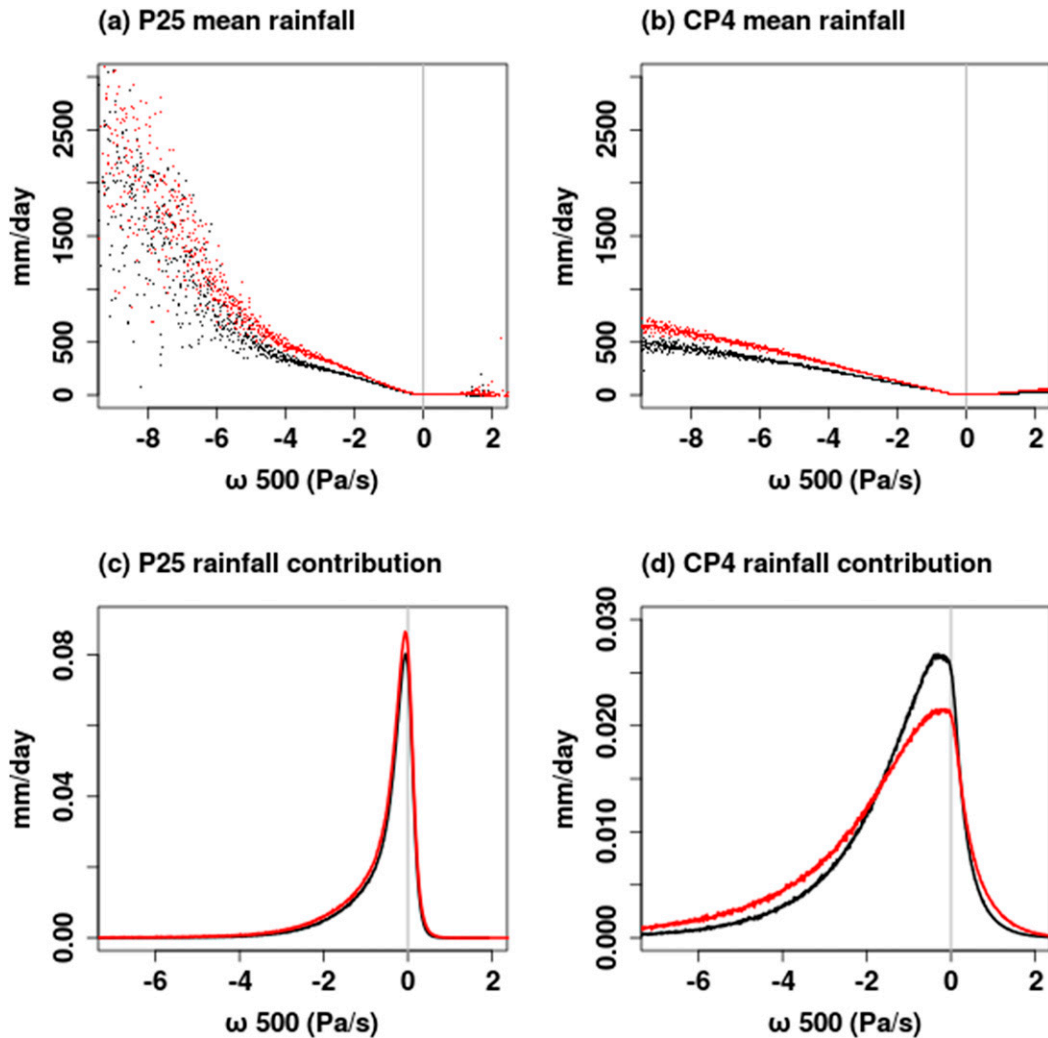


FIG. 11. (a) Composite mean rainfall for each vertical velocity (ω_{500}) data bin for P25. (b) As in (a), but for CP4. (c) Compositing contribution to mean rainfall for each ω_{500} data bin for P25. (d) As in (c), but for CP4. The integrated area under each contribution curve sums to the mean rainfall. Current climate is shown in black and future climate in red. Negative values for ω_{500} represent ascent and positive values descent. In (c) and (d), changes in the distributions of rainfall contribution by ω_{500} data bin under climate change are statistically significant at the 1% level.

the distribution of mean rainfall composited for each ω_{500} data bin (Figs. 11a,b). Composite mean rainfall is at a minimum at $\sim 0 \text{ Pa s}^{-1}$ and increases strongly with more intense ascent (with rain also associated with descent, presumably due to the role of rain in generating downdrafts). CP4 has less rainfall per unit ω_{500} than P25, which is compensated for by the propensity for more intense updrafts in CP4 than in P25. Under climate change, both P25 and CP4 show that composite mean rain intensity increases across the distribution of ω_{500} . This is due to the increase in TCW (Figs. 4 and 8).

Under climate change, the distribution of rainfall contribution composited by ω_{500} data bin for P25 shows

that increases in rainfall contribution in future climate are associated with weak ω_{500} updrafts, shown by the increase in peak contribution close to 0 Pa s^{-1} , and with a small increase $\sim -2 \text{ Pa s}^{-1}$ (Fig. 11c). In contrast, CP4 has a reduction in rainfall contribution associated with weak updrafts, an increase in contribution associated with relatively strong downdrafts, and an increase associated with updrafts exceeding $\sim -2 \text{ Pa s}^{-1}$ intensity (Fig. 11d).

The shift to more frequent intense updrafts in CP4 (Fig. 10d) suggests that dynamical changes play a key role in the intensification of extreme rainfall (Figs. 9d and 11d) and likely coupled through a positive feedback

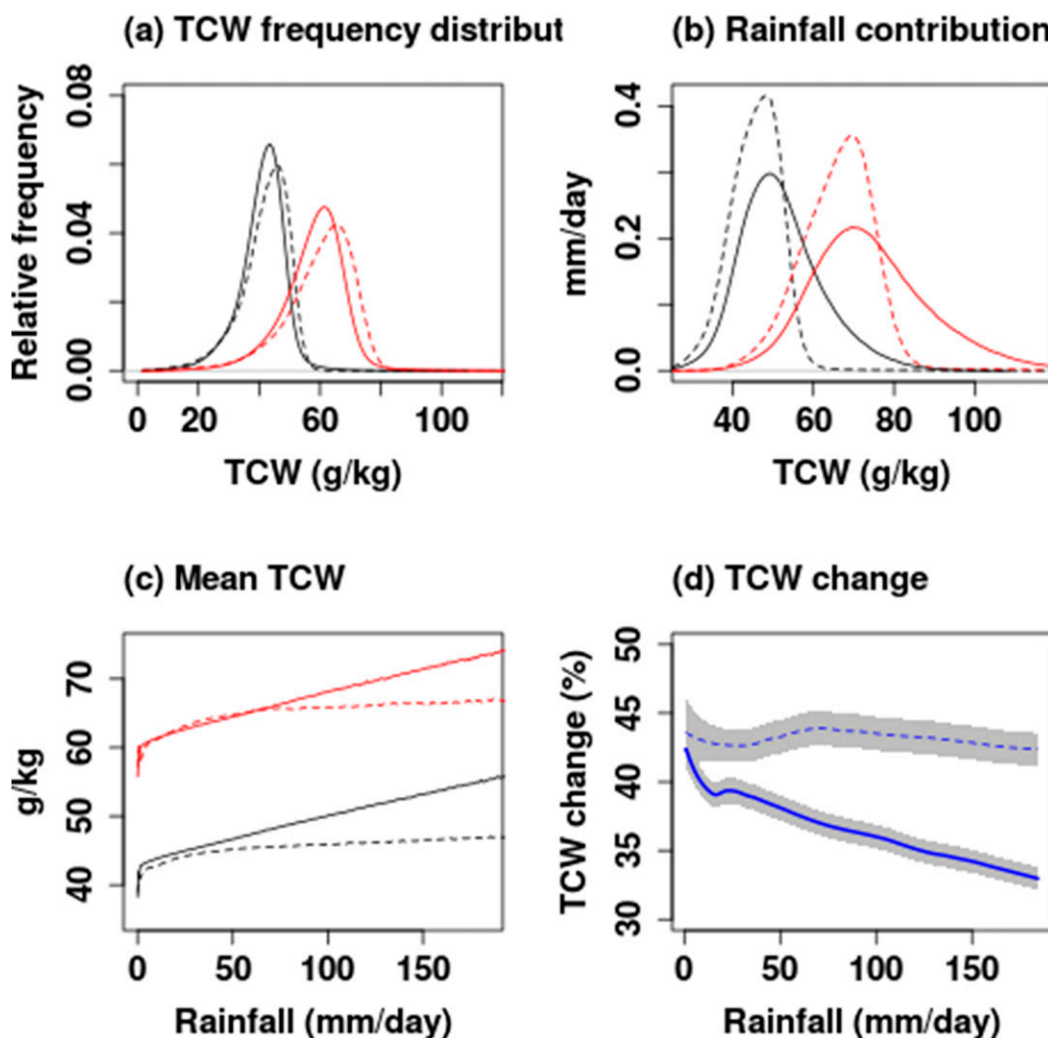


FIG. 12. (a) Relative frequency distribution of total column water (TCW). Changes in the distributions of P25 and CP4 under climate change and the differences between these changes are statistically significant at the 1% level. (b) Distribution of rainfall contribution composited by TCW data bin. The integrated area under each contribution curve sums to the mean rainfall. Changes in the distributions of rainfall contribution by TCW data bin under climate change are statistically significant at the 1% level. (c) Mean TCW composited by rainfall data bin. (d) Percentage change in mean TCW composited by rainfall data bin with the 95% confidence interval marked by gray shading. Current climate is shown in black, future climate in red, and climate change in blue. Dashed lines show results for P25 and solid lines results for CP4.

from enhanced latent heating during vertical motion (Pendergrass and Gerber 2016). In contrast, P25 is consistent with previous simulations using PCMs (e.g., Emori and Brown 2005) in showing that dynamical changes, represented by ω_{500} in this study (Fig. 10d), play a secondary role in changes to rain intensity (Figs. 9c and 11c). CMIP5 models project modest changes in mean rainfall and larger changes in extremes over Africa (Kitoh et al. 2013). The differences in the spatial patterns of rainfall change between P25 and CP4 (Fig. 2) and differences in the dynamical changes (Figs. 2, 8, and 10)

suggest that CMIP5 projections may overestimate the increase in mean rainfall and underestimate the intensification of wet and dry extremes over tropical Africa.

4) THE RELATIONSHIP BETWEEN RAINFALL AND TCW

In both P25 and CP4, the increases in TCW involve similar shifts in their frequency distributions toward greater TCW concentrations and similar increases in variance and skewness of the distributions (Fig. 12a). In both P25 and CP4, more intense rainfall is associated

with greater TCW as shown by the distribution of rainfall contribution composited for each TCW data bin (Fig. 12b). Despite their similar pdfs, in CP4 there is a far greater increase in the contribution to the total rain at high TCW (e.g., above 80 g kg^{-1}). This is consistent with the fact that positive anomalies of TCW are associated with positive anomalies in ascent, and ascent is intensified more in CP4. The association of more intense rainfall with greater TCW in CP4, however, holds at both heavier and lighter rain rates whereas in P25 the association is weak for rain intensity exceeding 50 mm day^{-1} (Fig. 12c).

Figure 12d shows the percentage change in the mean TCW composited for each rain intensity bin. There is a smaller increase in TCW at heavier rate intensities under climate change in CP4. In contrast, the increase in TCW in P25 is uniform across the range of rain intensities at $\sim 43\%$ (cf. Fig. 8d). This shows that, at relatively intense rain rates, a smaller increase in TCW is needed to give the same rain in CP4, consistent with the fact that updrafts intensify more in CP4 and that there is coupling between the changes in TCW and $\omega 500$ ascent.

When convection is resolved, there is an association of intense rainfall with positive TCW anomalies, which is consistent with observations of intense storms over West Africa (Taylor et al. 2017). In contrast, when convection is parameterized, the distributions of rainfall, TCW, and $\omega 500$ are more consistent with a climate of widespread, persistent light rainfall (Stephens et al. 2010) and there is weaker coupling between intense rainfall with high humidity.

4. Conclusions

Our results provide insight into how the response of convection and vertical motion to climate change differs when convection is resolved rather than parameterized. The CPM yielded more pronounced changes in the distribution of 3-hourly data and stronger coupling between changes in rainfall, vertical velocity, and humidity. These form the basis for contrasting changes in time-averaged mean climate between P25 and CP4.

Resolving convection gives similar spatial patterns of projected changes in annual mean rainfall, but the representation of convection remains a source of uncertainty, with correlations of projected annual changes in rainfall between explicit and parameterized convection of 0.60 and 0.77 (on 25- and 150-km grid scales, respectively). Under climate change, mean changes within the rain belt in P25 and CP4 show that rainfall becomes less frequent (Fig. 8), mean intensity (and mean rainfall) increases (Fig. 8), mean $\omega 500$ ascent weakens (Fig. 8), and TCW increases (Fig. 8). Compared to P25, CP4 has a greater reduction in rain frequency, a smaller increase in

mean rainfall, a greater weakening of mean $\omega 500$ ascent, and a pronounced increase in the occurrence of strong updrafts. The explicit resolution of convection in CP4, therefore, suggests that CMIP5 projections may overestimate the increase in mean rainfall, underestimate the intensification of wet and dry extremes over tropical Africa, and underestimate Hadley slowdown.

Crucially, the mean changes mask fundamental changes in the underlying frequency distributions of 3-hourly rainfall and vertical motion and mask marked differences between P25 and CP4. These key findings are summarized in schematic form in Fig. 13. It reveals the fundamental differences in behavior between P25 and CP4, especially since TCW and rainfall both respond to subgrid transport from the convection scheme, which is not measured directly using $\omega 500$. Figure 13 shows that there are couplings between the distributions of $\omega 500$, TCW, and rainfall that are absent from, or weakly captured in, P25. In CP4 (Figs. 13c,d), the contours of rain intensity (shown by the rows of blue circles of the same size) have a negative slope. Rainfall at a given intensity can be produced by weaker rates of ascent at times of higher TCW. In contrast, the rows of blue circles for P25 (Figs. 13a,b) are relatively flat, indicating that rain intensity is strongly associated with $\omega 500$, weakly associated with TCW, and not dependent on the joint distribution of $\omega 500$ and TCW. The explicit treatment of convection in CP4 yields stronger interactions between $\omega 500$, TCW, and rainfall, and a more pronounced shift to strong updrafts. In CP4, intense updrafts are linked to anomalously high TCW that may promote greater weakening of mean ascent and increased rainfall for less mean ascent. The differences in vertical velocity between the simulations and the largest changes in vertical velocity with climate change occur above the 500-hPa level (Fig. 7). A similar analysis using vertical velocity at 400 hPa (not shown) produced similar results and substantiates our conclusions.

This study describes results from the first pan-Africa scale convection-permitting simulations (Stratton et al. 2018) and consequently are based on a single climate realization from one climate model. Future work that replicates CP4 and P25 producing an ensemble of simulations would advance the findings of this study by enabling more robust quantification of uncertainty. Similarly, replication of CP4 and P25 using other climate models would provide deeper insight into our findings and further understanding of uncertainties.

We find that resolving convection in a climate model adds value to the simulation of future climate over Africa, specifically through the closer coupling of rainfall, vertical velocity, and TCW. Our results demonstrate that changes in future rainfall and dynamics, from the kilometer grid scale to the continental scale, are

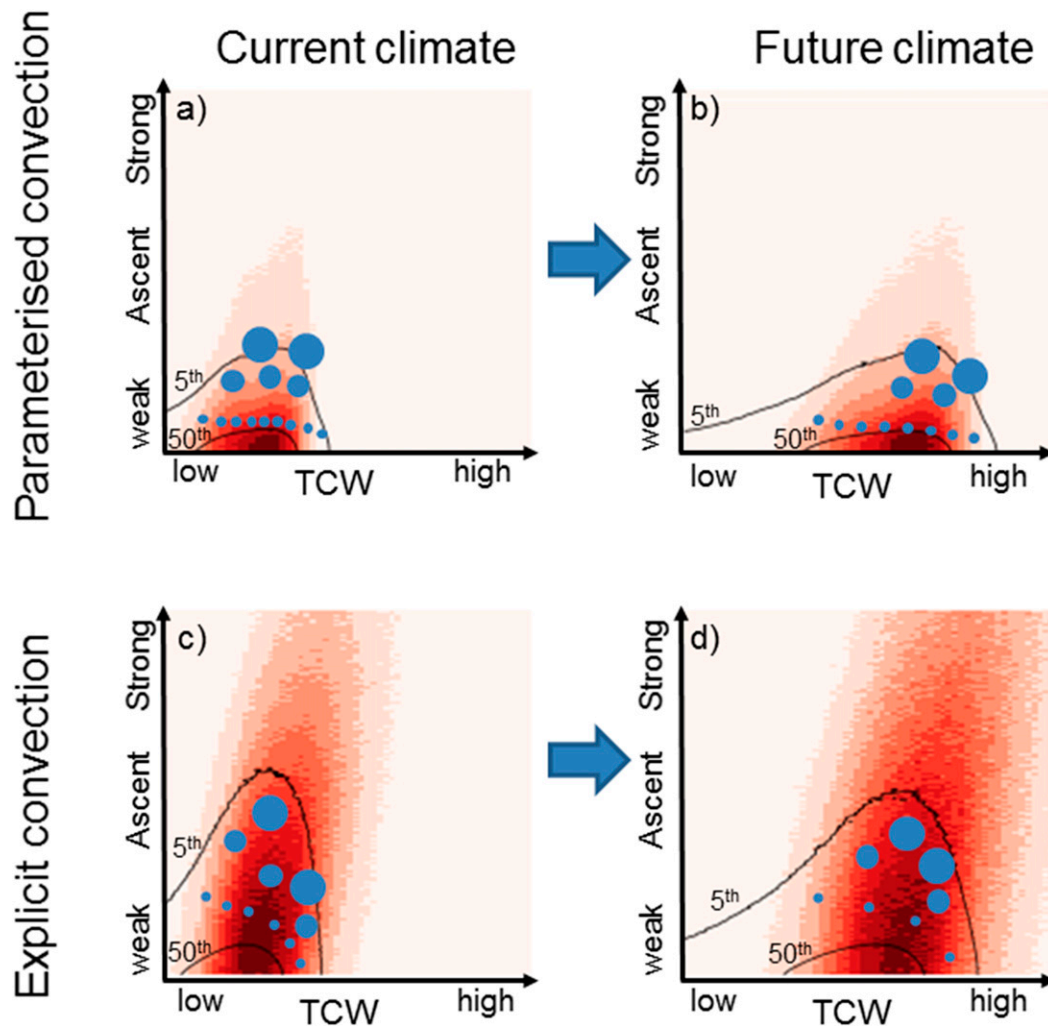


FIG. 13. The distribution of rainfall and its relationships with ascent and total column water (TCW). The colored pixels represent the joint density of rainfall contribution for ascent and TCW with darker colors representing larger contributions to rainfall. The black contour lines represent the 5th and 50th percentiles for the joint pdf of ascent and TCW. The blue circles represent rainfall with the size of the circles proportional to rain intensity and the number of circles proportional to rain frequency. The circles are positioned along contours of rate intensity and the allocation of the circles between the three contour lines was determined using relative frequencies of rainfall at each rate of intensity. With parameterized convection: (a) in current climate rainfall occurs frequently above a minimum threshold in TCW and at relatively weak ascent; (b) in future climate the rainfall distribution shifts to the right. Rainfall becomes less frequent and more intense and remains weakly linked to stronger ascent and higher TCW. With explicit convection: (c) in current climate rain intensity is more clearly associated with stronger ascent and higher TCW; and (d) in future climate this relationship reinforces the reduced frequency and increased intensity of rainfall. With explicit convection, rain intensity at a given rate of ascent increases with increasing TCW.

sensitive to the treatment of convection in climate models and not only in regions of tropical ascent but also in regions of subtropical climatological descent. The distributions of 3-hourly rainfall, vertical velocity, and TCW are sensitive to the treatment of convection and are influential for projected changes in mean state under climate change. These differences in the atmospheric circulation, and in rainfall frequency and intensity, are

likely to have major implications for planning adaptation to future climate warming.

Acknowledgments. The authors were supported by Natural Environment Research Council/Department for International Development (NERC/DFID, NE/MO17176/1, NE/M017214/1, and NE/M02038X/1) via the Future Climate for Africa (FCFA) funded projects: Improving

Model Processes for African Climate (IMPALA) and Integrating Hydro-Climatology Science into Policy Decisions for Climate-Resilient Infrastructure and Livelihoods in East Africa (HyCRISTAL). Jackson and Marsham were also supported by the DACCIWA project. DACCIWA funding from the European Union Seventh Framework Programme (FP7/2007–13) under Grant Agreement 603502 (EU project DACCIWA: Dynamics–Aerosol–Chemistry–Cloud Interactions in West Africa). Jackson was also supported by the AMMA-2050 project NE/M020126/1. Kendon gratefully acknowledges funding from the Joint U.K. BEIS/Defra Met Office Hadley Centre Climate Programme (GA01101). Marsham was also supported by the NCAS via the NERC/GCRF programme ACREW: Atmospheric Hazard in Developing Countries: Risk Assessment and Early Warning. Parker was supported by a Royal Society Wolfson Research Merit Award. We thank Malcolm Roberts (U.K. Met Office) for running the N512-resolution AMIP global simulation and Peter Willetts for help in processing TRMM data. We acknowledge the NASA/Goddard Space Flight Center’s Precipitation Measurement Missions and PPS for provision of the TRMM 3B42 version 7 dataset; and ECMWF for the ERA-Interim dataset. A sample of the CP4A dataset generated under the FCFA IMPALA project is publicly available from the Centre for Environmental Data Analysis (CEDA) archive (<http://archive.ceda.ac.uk/>). Finally, we thank two anonymous reviewers for their comments which greatly improved the paper.

REFERENCES

- Allen, M. R., and W. J. Ingram, 2002: Constraints on future changes in climate and the hydrologic cycle. *Nature*, **419**, 228–232, <https://doi.org/10.1038/NATURE01092>.
- Biasutti, M., 2013: Forced Sahel rainfall trends in the CMIP5 archive. *J. Geophys. Res. Atmos.*, **118**, 1613–1623, <https://doi.org/10.1002/JGRD.50206>.
- Birch, C. E., J. H. Marsham, D. J. Parker, and C. M. Taylor, 2014a: The scale dependence and structure of convergence fields preceding the initiation of deep convection. *Geophys. Res. Lett.*, **41**, 4769–4776, <https://doi.org/10.1002/2014GL060493>.
- , D. J. Parker, J. H. Marsham, D. Copsey, and L. Garcia-Carreras, 2014b: A seamless assessment of the role of convection in the water cycle of the West African monsoon. *J. Geophys. Res. Atmos.*, **119**, 2890–2912, <https://doi.org/10.1002/2013JD020887>.
- Bony, S., J.-L. Dufresne, H. Le Treut, J.-J. Morcrette, and C. Senior, 2004: On dynamic and thermodynamic components of cloud changes. *Climate Dyn.*, **22**, 71–86, <https://doi.org/10.1007/s00382-003-0369-6>.
- Byrne, M. P., and T. Schneider, 2016: Narrowing of the ITCZ in a warming climate: Physical mechanisms. *Geophys. Res. Lett.*, **43**, 11 350–11 357, <https://doi.org/10.1002/2016GL070396>.
- , and P. A. O’Gorman, 2018: Trends in continental temperature and humidity directly linked to ocean warming. *Proc. Natl. Acad. Sci. USA*, **115**, 4863–4868, <https://doi.org/10.1073/pnas.1722312115>.
- , A. G. Pendergrass, A. D. Rapp, and K. R. Wodzicki, 2018: Response of the intertropical convergence zone to climate change: Location, width, and strength. *Curr. Climate Change Rep.*, **4**, 355–370, <https://doi.org/10.1007/s40641-018-0110-5>.
- Chadwick, R., I. Boutle, and G. Martin, 2013: Spatial patterns of precipitation change in CMIP5: Why the rich do not get richer in the tropics. *J. Climate*, **26**, 3803–3822, <https://doi.org/10.1175/JCLI-D-12-00543.1>.
- , P. Good, T. Andrews, and G. Martin, 2014: Surface warming patterns drive tropical rainfall pattern responses to CO₂ forcing on all timescales. *Geophys. Res. Lett.*, **41**, 610–615, <https://doi.org/10.1002/2013GL058504>.
- Chou, C., and C.-A. Chen, 2010: Depth of convection and the weakening of tropical circulation in global warming. *J. Climate*, **23**, 3019–3030, <https://doi.org/10.1175/2010JCLI3383.1>.
- , —, P.-H. Tan, and K. T. Chen, 2012: Mechanisms for global warming impacts on precipitation frequency and intensity. *J. Climate*, **25**, 3291–3306, <https://doi.org/10.1175/JCLI-D-11-00239.1>.
- Christensen, J. H., and Coauthors, 2013: Climate phenomena and their relevance for future regional climate change. *Climate Change 2013: The Physical Science Basis*, T. F. Stocker et al., Eds., Cambridge University Press, 1217–1308.
- Clark, P., N. Roberts, H. Lean, S. P. Ballard, and C. Charlton-Perez, 2016: Convection-permitting models: A step-change in rainfall forecasting. *Meteor. Appl.*, **23**, 165–181, <https://doi.org/10.1002/met.1538>.
- Collins, M., and Coauthors, 2013: Long-term climate change: Projections, commitments and irreversibility. *Climate Change 2013: The Physical Science Basis*, T. F. Stocker et al., Eds., Cambridge University Press, 1029–1136.
- Crook, J., C. Klein, S. Folwell, C. M. Taylor, D. J. Parker, R. Stratton, and T. Stein, 2019: Assessment of the representation of West African storm lifecycles in convection-permitting simulations. *Earth Space Sci.*, **6**, 818–835, <https://doi.org/10.1029/2018EA000491>.
- Davies, T., 2014: Lateral boundary conditions for limited area models. *Quart. J. Roy. Meteor. Soc.*, **140**, 185–196, <https://doi.org/10.1002/qj.2127>.
- Dunning, C. M., E. Black, and R. P. Allan, 2018: Later wet seasons with more intense rainfall over Africa under future climate change. *J. Climate*, **31**, 9719–9738, <https://doi.org/10.1175/JCLI-D-18-0102.1>.
- Emori, S., and S. J. Brown, 2005: Dynamic and thermodynamic changes in mean and extreme precipitation under changed climate. *Geophys. Res. Lett.*, **32**, L17706, <https://doi.org/10.1029/2005GL023272>.
- Field, P. R., and Coauthors, 2017: Exploring the convective grey zone with regional simulations of a cold air outbreak. *Quart. J. Roy. Meteor. Soc.*, **143**, 2537–2555, <https://doi.org/10.1002/qj.3105>.
- Finney, D. L., and Coauthors, 2019: Implications of improved representation of convection for the East Africa water budget using a convection-permitting model. *J. Climate*, **32**, 2109–2129, <https://doi.org/10.1175/JCLI-D-18-0387.1>.
- Gochis, D. J., W. J. Shuttleworth, and Z.-L. Yang, 2002: Sensitivity of the modeled North American monsoon regional climate to convective parameterization. *Mon. Wea. Rev.*, **130**, 1282–1298, [https://doi.org/10.1175/1520-0493\(2002\)130<1282:SOTMNA>2.0.CO;2](https://doi.org/10.1175/1520-0493(2002)130<1282:SOTMNA>2.0.CO;2).
- Gregory, D., and P. R. Rowntree, 1990: A mass flux convection scheme with representation of cloud ensemble characteristics and stability-dependent closure. *Mon. Wea. Rev.*, **118**, 1483–1506, [https://doi.org/10.1175/1520-0493\(1990\)118<1483:AMFCSW>2.0.CO;2](https://doi.org/10.1175/1520-0493(1990)118<1483:AMFCSW>2.0.CO;2).
- Hart, N. C. G., R. Washington, and R. A. Stratton, 2018: Stronger local overturning in convective-permitting regional climate

- model improves simulation of the subtropical annual cycle. *Geophys. Res. Lett.*, **45**, 11 334–11 342, <https://doi.org/10.1029/2018GL079563>.
- , —, and R. I. Maidment, 2019: Deep convection over Africa: Annual cycle, ENSO, and trends in the hotspots. *J. Climate*, **32**, 8791–8811, <https://doi.org/10.1175/JCLI-D-19-0274.1>.
- Held, I. M., and B. J. Soden, 2006: Robust responses of the hydrological cycle to global warming. *J. Climate*, **19**, 5686–5699, <https://doi.org/10.1175/JCLI3990.1>.
- Hill, S. A., Y. Ming, I. M. Held, and M. Zhao, 2017: A moist static energy budget–based analysis of the sahel rainfall response to uniform oceanic warming. *J. Climate*, **30**, 5637–5660, <https://doi.org/10.1175/JCLI-D-16-0785.1>.
- Huffman, G. J., R. F. Adler, D. T. Bolvin, and E. J. Nelkin, 2010: The TRMM Multi-Satellite Precipitation Analysis (TMPA). *Satellite Rainfall Applications for Surface Hydrology*, M. Gebremichael and F. Hossain, Eds., Springer, 3–22.
- Joshi, M. M., J. M. Gregory, M. J. Webb, D. M. H. Sexton, and T. C. Johns, 2008: Mechanisms for the land/sea warming contrast exhibited by simulations of climate change. *Climate Dyn.*, **30**, 455–465, <https://doi.org/10.1007/s00382-007-0306-1>.
- Joyce, R. J., J. E. Janowiak, P. A. Arkin, and P. Xie, 2004: CMORPH: A method that produces global precipitation estimates from passive microwave and infrared data at high spatial and temporal resolution. *J. Hydrometeorol.*, **5**, 487–503, [https://doi.org/10.1175/1525-7541\(2004\)005<0487:CAMTPG>2.0.CO;2](https://doi.org/10.1175/1525-7541(2004)005<0487:CAMTPG>2.0.CO;2).
- Jury, M. R., 2016: Large scale features of Africa's diurnal climate. *Phys. Geogr.*, **37**, 120–131, <https://doi.org/10.1080/02723646.2016.1163004>.
- Kanji, G. K., 2006: *100 Statistical Tests*. SAGE Publications Ltd., 242 pp.
- Kendon, E. J., R. A. Stratton, S. Tucker, J. H. Marsham, S. Berthou, D. P. Rowell, and C. A. Senior, 2019: Enhanced future changes in wet and dry extremes over Africa at convection-permitting scale. *Nat. Commun.*, **10**, 1794, <https://doi.org/10.1038/s41467-019-09776-9>.
- Kitoh, A., H. Endo, K. K. Kumar, I. F. A. Cavalcanti, P. Goswami, and T. Zhou, 2013: Monsoons in a changing world: A regional perspective in a global context. *J. Geophys. Res. Atmos.*, **118**, 3053–3065, <https://doi.org/10.1002/JGRD.50258>.
- Knutson, T. R., and S. Manabe, 1995: Time-mean response over the tropical Pacific to increased CO₂ in a coupled ocean–atmosphere model. *J. Climate*, **8**, 2181–2199, [https://doi.org/10.1175/1520-0442\(1995\)008<2181:TMROTT>2.0.CO;2](https://doi.org/10.1175/1520-0442(1995)008<2181:TMROTT>2.0.CO;2).
- Kooperman, G. J., M. S. Pritchard, M. A. Burt, M. D. Branson, and D. A. Randall, 2016: Impacts of cloud superparameterization on projected daily rainfall intensity climate changes in multiple versions of the Community Earth System Model. *J. Adv. Model. Earth Syst.*, **8**, 1727–1750, <https://doi.org/10.1002/2016MS000715>.
- Koster, R. D., and Coauthors, 2004: Regions of strong coupling between soil moisture and precipitation. *Science*, **305**, 1138–1140, <https://doi.org/10.1126/science.1100217>.
- Lau, W. K. M., and K.-M. Kim, 2015: Robust Hadley circulation changes and increasing global dryness due to CO₂ warming from CMIP5 model projections. *Proc. Natl. Acad. Sci. USA*, **112**, 3630–3635, <https://doi.org/10.1073/pnas.1418682112>.
- Leroux, M., 1998: *Dynamic Analysis of Weather and Climate: Atmospheric Circulations, Perturbations, Climatic Evolution*. Wiley, 365 pp.
- Lock, A. P., A. R. Brown, M. R. Bush, G. M. Martin, and R. N. B. Smith, 2000: A new boundary layer mixing scheme. Part I: Scheme description and single-column model tests. *Mon. Wea. Rev.*, **128**, 3187–3199, [https://doi.org/10.1175/1520-0493\(2000\)128<3187:ANBLMS>2.0.CO;2](https://doi.org/10.1175/1520-0493(2000)128<3187:ANBLMS>2.0.CO;2).
- Ma, J., S.-P. Xie, and Y. Kosaka, 2012: Mechanisms for tropical tropospheric circulation change in response to global warming. *J. Climate*, **25**, 2979–2994, <https://doi.org/10.1175/JCLI-D-11-00048.1>.
- , R. Chadwick, K.-H. Seo, C. Dong, G. Huang, G. R. Foltz, and J. H. Jiang, 2018: Responses of the tropical atmospheric circulation to climate change and connection to the hydrological cycle. *Annu. Rev. Earth Planet. Sci.*, **46**, 549–580, <https://doi.org/10.1146/annurev-earth-082517-010102>.
- Mapes, B. E., 2001: Water's two height scales: The moist adiabat and the radiative troposphere. *Quart. J. Roy. Meteor. Soc.*, **127**, 2353–2366, <https://doi.org/10.1002/qj.49712757708>.
- Marsham, J. H., N. S. Dixon, L. Garcia-Carreras, G. M. S. Lister, D. J. Parker, P. Knippertz, and C. E. Birch, 2013: The role of moist convection in the West African monsoon system: Insights from continental-scale convection-permitting simulations. *Geophys. Res. Lett.*, **40**, 1843–1849, <https://doi.org/10.1002/grl.50347>.
- McGregor, G. R., and S. Nieuwolt, 1998: *Tropical Climatology: An Introduction to the Climates of the Low Latitudes*. John Wiley & Sons, 352 pp.
- Moss, R. H., and Coauthors, 2010: The next generation of scenarios for climate change research and assessment. *Nature*, **463**, 747–756, <https://doi.org/10.1038/nature08823>.
- NASA, 2015: Tropical Rainfall Measuring Mission brightness temperature and 3B42 precipitation product, version 7. NASA Goddard Earth Sciences Data and Information Service Center, accessed 28 August 2014, http://disc.sci.gsfc.nasa.gov/precipitation/documentation/TRMM_README/TRMM_3B42_readme.shtml.
- Niang, I., O. C. Ruppel, M. A. Abdrabo, A. Essel, C. Lennard, J. Padgham, and P. Urquhart, 2014: Africa. *Climate Change 2014: Impacts, Adaptation, and Vulnerability. Part B: Regional Aspects*, V. R. Barros et al., Eds., Cambridge University Press, 1199–1265.
- Nicholson, S. E., 2009: A revised picture of the structure of the “monsoon” and land ITCZ over West Africa. *Climate Dyn.*, **32**, 1155–1171, <https://doi.org/10.1007/s00382-008-0514-3>.
- , 2018: The ITCZ and the seasonal cycle over equatorial Africa. *Bull. Amer. Meteor. Soc.*, **99**, 337–348, <https://doi.org/10.1175/BAMS-D-16-0287.1>.
- Nikulin, G., and Coauthors, 2012: Precipitation climatology in an ensemble of CORDEX-Africa regional climate simulations. *J. Climate*, **25**, 6057–6078, <https://doi.org/10.1175/JCLI-D-11-00375.1>.
- O’Gorman, P. A., and C. J. Muller, 2010: How closely do changes in surface and column water vapor follow Clausius–Clapeyron scaling in climate change simulations? *Environ. Res. Lett.*, **5**, 025207, <https://doi.org/10.1088/1748-9326/5/2/025207>.
- Pearson, K. J., G. M. S. Lister, C. E. Birch, R. P. Allan, R. J. Hogan, and S. J. Woolnough, 2014: Modelling the diurnal cycle of tropical convection across the ‘grey zone’. *Quart. J. Roy. Meteor. Soc.*, **140**, 491–499, <https://doi.org/10.1002/qj.2145>.
- Pendergrass, A. G., and E. P. Gerber, 2016: The rain is askew: Two idealized models relating vertical velocity and precipitation distributions in a warming world. *J. Climate*, **29**, 6445–6462, <https://doi.org/10.1175/JCLI-D-16-0097.1>.
- Pielke, R. A., Sr., 2002: *Mesoscale Meteorological Modeling*. 2nd ed. Academic Press, 676 pp.
- Prein, A. F., and Coauthors, 2015: A review on regional convection-permitting climate modeling: Demonstrations, prospects, and challenges. *Rev. Geophys.*, **53**, 323–361, <https://doi.org/10.1002/2014RG000475>.
- Raghavendra, A., L. Zhou, Y. Jiang, and W. Hua, 2018: Increasing extent and intensity of thunderstorms observed over the

- Congo Basin from 1982 to 2016. *Atmos. Res.*, **213**, 17–26, <https://doi.org/10.1016/j.atmosres.2018.05.028>.
- Reynolds, R. W., T. M. Smith, C. Liu, D. B. Chelton, K. S. Casey, and M. G. Schlax, 2007: Daily high-resolution-blended analyses for sea surface temperature. *J. Climate*, **20**, 5473–5496, <https://doi.org/10.1175/2007JCLI1824.1>.
- Riehl, H., and J. S. Malkus, 1958: On the heat balance in the equatorial trough zone. *Geophysica*, **6**, 503–537.
- Scannell, C., and Coauthors, 2019: The influence of remote aerosol forcing from industrialized economies on the future evolution of East and West African rainfall. *J. Climate*, **32**, 8335–8354, <https://doi.org/10.1175/JCLI-D-18-0716.1>.
- Schumacher, C., and R. A. Houze Jr., 2003: Stratiform rain in the tropics as seen by the TRMM precipitation radar. *J. Climate*, **16**, 1739–1756, [https://doi.org/10.1175/1520-0442\(2003\)016<1739:SRITTA>2.0.CO;2](https://doi.org/10.1175/1520-0442(2003)016<1739:SRITTA>2.0.CO;2).
- Seth, A., A. Giannini, M. Rojas, S. A. Rauscher, S. Bordoni, D. Singh, and S. J. Camargo, 2019: Monsoon responses to climate changes—Connecting past, present and future. *Curr. Climate Change Rep.*, **5**, 63–79, <https://doi.org/10.1007/s40641-019-00125-y>.
- Sherwood, S. C., S. Bony, and J.-L. Dufresne, 2014: Spread in model climate sensitivity traced to atmospheric convective mixing. *Nature*, **505**, 37–42, <https://doi.org/10.1038/nature12829>.
- Singh, M. S., and P. A. O’Gorman, 2015: Increases in moist-convective updraught velocities with warming in radiative-convective equilibrium. *Quart. J. Roy. Meteor. Soc.*, **141**, 2828–2838, <https://doi.org/10.1002/qj.2567>.
- Smith, R. N. B., 1990: A scheme for predicting layer clouds and their water content in a general circulation model. *Quart. J. Roy. Meteor. Soc.*, **116**, 435–460, <https://doi.org/10.1002/qj.49711649210>.
- Stein, T. H. M., and Coauthors, 2019: An evaluation of clouds and precipitation in convection-permitting forecasts for South Africa. *Wea. Forecasting*, **34**, 233–254, <https://doi.org/10.1175/WAF-D-18-0080.1>.
- Stephens, G. L., and Coauthors, 2010: Dreary state of precipitation in global models. *J. Geophys. Res.*, **115**, D24211, <https://doi.org/10.1029/2010JD014532>.
- Stratton, R., and Coauthors, 2018: A pan-African convection-permitting regional climate simulation with the Met Office Unified Model: CP4-Africa. *J. Climate*, **31**, 3485–3508, <https://doi.org/10.1175/JCLI-D-17-0503.1>.
- Suzuki, T., 2011: Seasonal variation of the ITCZ and its characteristics over central Africa. *Theor. Appl. Climatol.*, **103**, 39–60, <https://doi.org/10.1007/s00704-010-0276-9>.
- Taylor, C. M., C. E. Birch, D. J. Parker, N. Dixon, F. Guichard, G. Nikulin, and G. M. S. Lister, 2013: Modeling soil moisture–precipitation feedback in the Sahel: Importance of spatial scale versus convective parameterization. *Geophys. Res. Lett.*, **40**, 6213–6218, <https://doi.org/10.1002/2013GL058511>.
- , and Coauthors, 2017: Frequency of extreme Sahelian storms tripled since 1982 in satellite observations. *Nature*, **544**, 475–478, <https://doi.org/10.1038/nature22069>.
- Vecchi, G. A., and B. J. Soden, 2007: Global warming and the weakening of the tropical circulation. *J. Climate*, **20**, 4316–4340, <https://doi.org/10.1175/JCLI4258.1>.
- Waliser, D. E., and C. Gautier, 1993: A satellite-derived climatology of the ITCZ. *J. Climate*, **6**, 2162–2174, [https://doi.org/10.1175/1520-0442\(1993\)006<2162:ASDCOT>2.0.CO;2](https://doi.org/10.1175/1520-0442(1993)006<2162:ASDCOT>2.0.CO;2).
- Walters, D. N., and Coauthors, 2017: The Met Office Unified Model Global Atmosphere 6.0/6.1 and JULES Global Land 6.0/6.1 configurations. *Geosci. Model Dev.*, **10**, 1487–1520, <https://doi.org/10.5194/gmd-10-1487-2017>.
- , and Coauthors, 2019: The Met Office Unified Model Global Atmosphere 7.0/7.1 and JULES Global Land 7.0 configurations. *Geosci. Model Dev.*, **12**, 1909–1963, <https://doi.org/10.5194/gmd-12-1909-2019>.
- White, B., A. Buchanan, C. Birch, P. Stier, and K. Pearson, 2018: Quantifying the effects of horizontal grid length and parameterized convection on the degree of convective organization using a metric of the potential for convective interaction. *J. Atmos. Sci.*, **75**, 425–450, <https://doi.org/10.1175/JAS-D-16-0307.1>.
- Willets, P. D., J. H. Marsham, C. E. Birch, D. J. Parker, S. Webster, and J. Petch, 2017: Moist convection and its upscale effects in simulations of the Indian monsoon with explicit and parameterized convection. *Quart. J. Roy. Meteor. Soc.*, **143**, 1073–1085, <https://doi.org/10.1002/qj.2991>.
- Williams, K. T., and W. M. Gray, 1973: Statistical analysis of satellite-observed trade wind cloud clusters in the western North Pacific. *Tellus*, **4**, 313–336, <https://doi.org/10.3402/TELLUSA.V25I4.9667>.
- Wilson, D. R., A. C. Bushell, A. M. Kerr-Munslow, J. D. Price, and C. J. Morcrette, 2008: PC2: A prognostic cloud fraction and condensation scheme. I: Scheme description. *Quart. J. Roy. Meteor. Soc.*, **134**, 2093–2107, <https://doi.org/10.1002/qj.333>.
- Wood, N., and Coauthors, 2014: An inherently mass-conserving semi-implicit semi-Lagrangian discretization of the deep-atmosphere global non-hydrostatic equations. *Quart. J. Roy. Meteor. Soc.*, **140**, 1505–1520, <https://doi.org/10.1002/qj.2235>.
- Woodhams, B. J., C. E. Birch, J. H. Marsham, C. L. Bain, N. M. Roberts, and D. F. A. Boyd, 2018: What is the added value of a convection-permitting model for forecasting extreme rainfall over tropical East Africa? *Mon. Wea. Rev.*, **146**, 2757–2780, <https://doi.org/10.1175/MWR-D-17-0396.1>.
- Xie, P., R. Joyce, S. Wu, S.-H. Yoo, Y. Yarosh, F. Sun, and R. Lin, 2017: Reprocessed, bias-corrected CMORPH global high-resolution precipitation estimates from 1998. *J. Hydrometeorol.*, **18**, 1617–1641, <https://doi.org/10.1175/JHM-D-16-0168.1>.
- Yang, G.-Y., and J. Slingo, 2001: The diurnal cycle in the tropics. *Mon. Wea. Rev.*, **129**, 784–801, [https://doi.org/10.1175/1520-0493\(2001\)129<0784:TDCITT>2.0.CO;2](https://doi.org/10.1175/1520-0493(2001)129<0784:TDCITT>2.0.CO;2).
- Zhou, L., and Coauthors, 2014: Widespread decline of Congo rainforest greenness in the past decade. *Nature*, **509**, 86–90, <https://doi.org/10.1038/nature13265>.
- Zipser, E. L., 1969: The role of organized unsaturated convective downdrafts in the structure and rapid decay of an equatorial disturbance. *J. Appl. Meteor.*, **8**, 799–814, [https://doi.org/10.1175/1520-0450\(1969\)008<0799:TROUC>2.0.CO;2](https://doi.org/10.1175/1520-0450(1969)008<0799:TROUC>2.0.CO;2).